Nucleic Acids Research, 2021 **1**
doi: 10.1093/nar/gkab252

Cistrome analysis of YY1 uncovers a regulatory axis of YY1:BRD2/4-PFKP during tumorigenesis of advanced prostate cancer

Chenxi Xu[1,2], Yi-Hsuan Tsai[1], Phillip M. Galbo, Jr.[3], Weida Gong[1], Aaron J. Storey[4], Yuemei Xu[5,6], Stephanie D. Byrum[4], Lingfan Xu[5], Young E. Whang[1,7,8], Joel S. Parker[1,9], Samuel G. Mackintosh[4], Ricky D. Edmondson[4], Alan J. Tackett[4], Jiaoti Huang[5], Deyou Zheng[3,10], H. Shelton Earp[1,7,11], Gang Greg Wang[1,2,11,*] and Ling Cai[1,9,*]

[1]Lineberger Comprehensive Cancer Center, University of North Carolina at Chapel Hill School of Medicine, Chapel Hill, NC 27599, USA, [2]Department of Biochemistry and Biophysics, University of North Carolina at Chapel Hill School of Medicine, Chapel Hill, NC 27599, USA, [3]Department of Genetics, Albert Einstein College of Medicine, Bronx, NY 10461, USA, [4]Department of Biochemistry and Molecular Biology, University of Arkansas for Medical Sciences, Little Rock, AR 72205, USA, [5]Department of Pathology, Duke University School of Medicine, Durham, NC 27710, USA, [6]Department of Pathology, Nanjing Drum Tower Hospital and The Affiliated Hospital of Nanjing University Medical School, Nanjing, 210008, China, [7]Department of Medicine, University of North Carolina at Chapel Hill School of Medicine, Chapel Hill, NC, 27599, USA, [8]Department of Pathology and Laboratory Medicine, University of North Carolina at Chapel Hill School of Medicine, Chapel Hill, NC, 27599, USA, [9]Department of Genetics, University of North Carolina at Chapel Hill School of Medicine, Chapel Hill, NC 27599, USA, [10]Department of Neurology and Department of Neuroscience, Albert Einstein College of Medicine, Bronx, NY 10461, USA and [11]Department of Pharmacology, University of North Carolina at Chapel Hill School of Medicine, Chapel Hill, NC, 27599, USA

Received February 12, 2021; Editorial Decision March 25, 2021; Accepted March 26, 2021

ABSTRACT

Castration-resistant prostate cancer (CRPC) is a terminal disease and the molecular underpinnings of CRPC development need to be better understood in order to improve its treatment. Here, we report that a transcription factor Yin Yang 1 (YY1) is significantly overexpressed during prostate cancer progression. Functional and cistrome studies of YY1 uncover its roles in promoting prostate oncogenesis *in vitro* and *in vivo,* as well as sustaining tumor metabolism including the Warburg effect and mitochondria respiration. Additionally, our integrated genomics and interactome profiling in prostate tumor show that YY1 and bromodomain-containing proteins (BRD2/4) co-occupy a majority of gene-regulatory elements, coactivating downstream targets. Via gene loss-of-function and rescue studies and mutagenesis of YY1-bound cis-elements, we unveil an oncogenic pathway in which YY1 directly binds and activates *PFKP*, a gene encoding the rate-limiting enzyme for glycolysis, significantly contributing to the YY1-enforced Warburg effect and malignant growth. Altogether, this study supports a master regulator role for YY1 in prostate tumorigenesis and reveals a YY1:BRD2/4-PFKP axis operating in advanced prostate cancer with implications for therapy.

INTRODUCTION

Prostate cancer is the second leading cause of cancer-related death for men in the United States. Standard treatment of prostate cancer with anti-androgen agents fails inevitably due to development of therapy resistance and castration-resistant prostate cancer (CRPC), a terminal disease (1). Mechanistic understanding of CRPC pathogenesis and design of novel means to specifically target CRPC vulnerabilities would greatly benefit clinical outcome of the affected patients.

Yin Yang 1 (YY1), a transcription factor with four conserved C2H2 zinc fingers (2), was previously shown to have dual roles in gene activation and repression (3–5). As a multifunctional protein, YY1 is involved in various biological and physiological processes including cell proliferation, lineage specification, embryonic development and tumorigenesis (5–7). In this work, our analysis using a large set of nor-

*To whom correspondence should be addressed. Tel: +1 919 966 5953; Fax: +1 919 966 9673; Email: ling_cai@med.unc.edu
Correspondence may also be addressed to Greg Wang. Email: greg_wang@med.unc.edu

mal and patient samples demonstrates that YY1 expression is significantly increased during progression of advanced prostate cancer. However, YY1′s function and the regulated cistrome in this disease have not been studied.

Aerobic glycolysis, also known as the Warburg effect, is essential for cancer to acquire energy and metabolize nutrients for synthesis of macromolecular precursors, in order to sustain high rates of cell proliferation (8). It has been reported that prostate cancer is metabolically different from many other solid tumors due to an enhanced reliance on oxidative phosphorylation (OXPHOS) in mitochondria, leading to a modest level of glucose uptake (9,10). Other studies, however, have also shown increased glycolysis or the Warburg effect correlated with disease progression and poor prognosis of advanced prostate cancer (10). The exact molecular mechanisms underlying glycolysis regulation in advanced prostate tumors remain elusive, although rising evidence points to possible deregulation of glycolytic enzymes (11,12). In glycolysis, phosphofructokinase 1 (PFK1) is critical for catalyzing fructose 6-phosphate (F6P) to fructose 1,6-biphosphate (F1,6BP), a rate-limiting step for glycolysis (13). PFK1 has three isoforms, namely, PFKP (phosphofructokinase, platelet), PFKM (phosphofructokinase, muscle) and PFKL (phosphofructokinase, liver). While all isozymes are expressed in many tissues, PFKP and PFKM are mainly present in platelet and muscle, respectively, whereas PFKL is predominant in liver and kidney (14). The functional role of PFKP or its regulation in prostate cancer is unexplored to date.

Here, we demonstrate that, in agreement with its significantly elevated level in advanced CRPC disease, YY1 is essential for CRPC tumorigenesis in multiple in vitro and in vivo CRPC models. Our integrative genomics and proteomics-based approaches (RNA-seq, ChIP-seq and interactome studies) determine the YY1-regulated cistrome in CRPC, and, strikingly, show that YY1 and its bromodomain-containing partners (BRD4) co-bind to a majority of cis-regulatory elements (demarcated by H3K27ac) in CRPC cells, potentiating gene-expression programs related to malignant growth and metabolic pathways such as the Warburg effect. Gene loss-of-function and rescue and cis-element mutational studies point to an oncogenic axis involving YY1-PFKP, which operates to enhance cell glycolysis and tumor growth. Altogether, this study shows YY1 acting as a master regulator of prostate tumorigenesis, unveils a previously unknown oncogenic pathway involving YY1:BRD4/2-PFKP, and elucidates the molecular mechanism underlying the altered metabolism of CRPC, implicative of new therapeutic strategies for the treatment of this lethal disease.

MATERIALS AND METHODS

Analysis of public prostate cancer datasets

Gene-expression datasets from the NCBI GEO accession numbers GSE68907, GSE6099 and GSE3325 were extracted, log2 transformed for each sample, and used for association analyses with sample types (such as benign, primary or metastatic) by analysis of variance (ANOVA) test.

Immunohistochemistry (IHC)

YY1 IHC staining was conducted using a rabbit anti-YY1 antibody (Atlas Antibodies #HPA001119) and the Bond fully automated slide staining system (Leica Microsystems). Slides were dewaxed in Bond Dewax solution (AR9222) and hydrated in Bond Wash solution (AR9590). Heat-induced antigen retrieval was performed for 30 min at 100°C in Bond-Epitope Retrieval solution 1 pH-6.0 (AR9961), followed with a 5-min Bond peroxide blocking step (DS9800). After pretreatment, slides were incubated for 30mins with primary antibody YY1(1:150) followed with Vector Immpress HRP anti-rabbit IgG (MP-7401-15). Chromogenic detection of all antibodies was performed using the Bond Intense R Detection kit (DS9263). Stained slides were dehydrated and covered with a slip. Positive and negative controls (no primary antibody) were included for each run. Stained slides were digitally scanned at 20x magnification using Aperio ScanScope-XT (Aperio Technologies, Vista, CA, USA). The images were uploaded to the Aperio eSlideManager database (Leica Biosystems Inc; eSlideManager version 12.3.3.7075) and scored by the Translational Pathology Laboratory at UNC.

Tissue microarray (TMA)

TMAs, produced by the Duke Pathology department, were subject to immunohistochemistry (IHC) staining of YY1, followed by evaluation in a blinded fashion by experienced pathologists. Scoring was assessed on the basis of staining intensity from 0 (no staining) to 3 (strong) and percentage of tumor cell expression (1 to 100%), creating a composite score from 0 to 300 for each sample.

Cell Lines

HEK293 and HEK293T cells (acquired from American Type Culture Collection, ATCC) were cultured in DMEM supplemented with 10% FBS and 1% antibiotics. The human prostate cancer cell lines, 22Rv1, C4-2 and LNCaP, were obtained from ATCC and grown in the RPMI-1640 base medium supplemented with 10% FBS and 1% antibiotics. For compound treatment experiments, cells were first cultured under ligand-starved conditions for three days using the phenol red-free RPMI-1640 base medium supplemented with 10% charcoal-stripped serum, followed by treatment with vehicle, dihydrotestosterone (DHT), or DHT together with other compounds. All cells were maintained at 37°C with 5% CO_2. Authentication of cell line identities, including those of parental and derived lines, was ensured by the Tissue Culture Facility (TCF) affiliated to UNC Lineberger Comprehensive Cancer Center with the genetic signature profiling and fingerprinting analysis. Every 1–2 months, a routine examination of cell lines in culture for any possible mycoplasma contamination was performed using commercially available detection kits (Lonza).

Virus production and stable cell line generation

Generation of the stable cell lines with gene knockdown was carried out by using the pLKO.1-puro-based lentiviral

shRNA system as described before (15). The shRNA plasmid and packaging vector (VSV-G and psPAX2) were co-transfected using Lipofectamine 3000 into 293FT cells. Viral supernatant was collected and filtered 48 h after transfection. Cells were infected for 48 h with virus in the presence of 8 μg/ml polybrene. Then, the infected cells were selected out with the appropriate antibiotics.

Chemicals

DHT is purchased from Sigma and the bromodomain inhibitor JQ1 were described before (16).

Antibodies

Antibodies used in the work included the rabbit antibodies against HA tag (Cell Signaling #C29F4), PFKP (Cell Signaling #5412S), beta-Actin (Cell Signaling #13E5), BRD4 (Bethyl Laboratories #A301-985A100), H3K27ac (Abcam #ab4729), cleaved caspase 3 and 7 (Cell Signaling #9664 and 8438), as well as the mouse antibodies against Flag tag (Sigma #F1804), YY1 (Santa Cruz #SC7341; for blotting), YY1 (Atlas Antibodies #HPA001119; for IHC), TADA2A (Active Motif #61334), and α-Tubulin (Sigma #T9026). Anti-FLAG M2 Magnetic Beads (Sigma #M8823) was obtained from Sigma and used for immunoprecipitation. HRP-linked secondary antibodies, either anti-mouse IgG (#7076S) or anti-rabbit IgG (#7074S), were obtained from Cell Signaling.

Plasmids

cDNAs of human YY1, PFKP, ENO2 and ALDOC were amplified by PCR using total RNAs of 22Rv1 cells, fused in-frame with a HA tag and then cloned into a lentiviral vector of pCDH-EF1α-MCS-IRES-Puro/Neo (System Biosciences, CD532A-2/CD533A-2). The YY1 mutations, 170–200_K→R (six lysines within the amino acids 170–200 all mutated to arginines; kindly provided by Dr Edward Seto, George Washington University Cancer Center), S365D and deletion of the amino acids 1–100, were produced by site-directed mutagenesis (Strategene) or PCR. A PGL3-based luciferase reporter with a PFKP promoter region (–2008 to +7) was previously described and kindly provided by Dr Kyung-Sup Kim (Yonsei University, Korea). The PFKP promoter (–575 to +37) region was cloned from gDNA by PCR from using primers (5′-AACTGCG GGGTTTCCACCCGCCCCG-3′ and 5′-AGGAGCCCT TGGGGGCCCGGGAGTC-3′), followed by insertion into the pGL3-basic vector (Promega). This PFKP promoter region (–575 to +37) with mutation of the YY1 motif sites was produced by site-directed mutagenesis (with the YY1 core motif sequence 5′-CCAT mutated to 5′-CGGT). The cDNA of wild-type (WT) BRD4 and its ΔBD mutant were provided by Dr. Qiang Zhou (UC Berkeley) and subcloned into a home-made pcDNA-3.1_Flag vector for transient expression. For the BioID-based protein interactome study, a biotin ligase (BirA) cDNA (a kind gift of Brian Strahl, UNC) was cloned into the home-made MSCV-puro retroviral vector and then a Flag-tagged YY1 cDNA was fused in-frame to C-terminus of BirA. All plasmids were confirmed by sequencing before use.

RNA interference-mediated gene knockdown (KD) and CRISPR/cas9-mediated gene depletion

YY1 ON-TARGETplus SMART-pool siRNA (L-011796-00-0005) and non-targeting control siRNA (D-001810-10-05) were purchased from Dharmacon RNAi Technologies. Lentiviral pLKO.1-based shRNA vectors for KD of human YY1 (TRCN0000019894 [sh#94] and TRCN0000019898 [sh#98]), PFKP (TRCN0000037775 [sh#75] and TRCN0000037777 [sh#77]) and BRD2 (TRCN0000006308 [sh#8] and TRCN0000006311 [sh#11]) were purchased from Sigma. The shRNAs against GFP and luciferase were used as control. As the YY1 shRNA#94 targets the 3′-UTR of YY1, we thus used the coding region of YY1 in our rescue experiment. The sgRNAs targeting YY1 were cloned into a pLenti_LRG-2.1_Neo vector (Addgene 125593). A lentiviral plasmid that allows the doxycycline-inducible expression of SpCas9 was obtained from Dr. David Sabatini. The sgRNA sequences for targeting YY1 are YY1_sg#1 (GTGGGCGGCGACGACTCGGA) and YY1_sg#2 (GTCGGGTCGTCGGTGACCAG). All plasmid sequences were verified by sequencing.

Cell proliferation assays

Three thousand cells per well were seeded in triplicate in 96-well plate for each time point. The changes in cell number were measured using MTT assay kit based on instruction of the manufacturer (Promega).

Colony formation assays

Cells were plated in triplicate at a density of 20,000 cells per well in the six-well plate and grew for 3 weeks before staining with iodonitrotetrazoliuim chloride solution (Sigma). Culture medium was changed twice a week.

Cell cycle progression

To measure cell cycle progression, cells were collected by centrifugation, washed in the ice-cold PBS and then fixed in the pre-chilled methanol (80%), followed by staining with PBS plus 20 μg/ml of propidium iodide (PI; Sigma), 0.1% of Triton-X100 and 200 μg/ml of RNase A (Roche). DNA contents were then detected with a CyAnADP flow cytometer (Beckman-Coulter), and then analyzed by the flowJo Software (BD).

Co-immunoprecipitation (Co-IP)

Briefly, the cell pellets were lysed in RIPA buffer supplemented with complete protease inhibitors (Roche) and PMSF. 1mg of protein from whole cell lysate was incubated with the antibodies on a rotator overnight at 4°. Then, 20 μl of protein G agarose beads (Roche, 11243233001) were added for an additional 2 h with rotation at 4°. The beads were washed with RIPA buffer for three times, resuspended in 40 μl of 2× protein loading buffer, and boiled at 95°C for 5 min before loading onto SDS-PAGE gel. Western blot was performed with standard protocols.

RNA-seq

RNA was prepared, and complementary DNA was generated, amplified and subjected for library construction using TruSeq RNA Library Preparation Kit v2 (Illumina; catalog# RS-122-2002) as described before (15,17,18). Multiplexed RNA-Seq libraries were subject to sequencing using Illumina Hi-Seq 2500/4000 (available at the UNC-Chapel Hill High-Throughput Sequencing Facility) according to manufacturer's instructions.

RNA-seq and data analysis

The fastq files were aligned to the GRCh38 human genome (GRCh38.d1.vd1.fa) using STAR v2.4.2 (19) with parameters: –outSAMtype BAM Unsorted –quantMode TranscriptomeSAM. Transcript abundance for each sample was estimated with salmon v0.1.19 (20) to quantify the transcriptome defined by Gencode v22. Gene level counts were summed across isoforms and genes with low counts (maximum expression < 10) were filtered for the downstream analyses. We tested genes for differential expression in DESeq2 (21) in R. Genes with the absolute value of fold-change (FC) over 1.50 and adjusted P value <0.01 between YY1 KD and control samples were called as differentially expressed genes (DEGs).

Real-time RT-PCR

Total RNA was isolated using the RNeasy Mini Kit (Qiagen). First strand cDNA was synthesized using the High-Capacity cDNA Reverse Transcription Kit (Applied Biosystems). Real-time PCR was performed in triplicate using the iTaq Universal SYBR Green master mix (Bio-Rad) and the Quant Studio 6 Flex Real-Time PCR System (Applied Biosystems). All values were normalized to those of beta-actin. Information of the used primers is listed in Supplementary Table S4.

ChIP-seq

ChIP-seq was carried out as before (15,17,18). Briefly, 22Rv1 cells were first cultured under a ligand-starved condition for three days, followed by a 6-h drug treatment with vehicle or 10nM of Dihydrotestosterone (DHT). Cells were cross-linked with 1% formaldehyde at room temperature for 10 min, followed by addition of glycine to stop crosslinking. After washing, lysis and sonication, the chromatin fraction was incubated with antibody-conjugated Dynabeads (Invitrogen) overnight at 4°C. Chromatin-bound beads were subject to extensive washing and elution. Eluted chromatin was de-crosslinked overnight at 65°C, followed by protein digestion with proteinase K and DNA purification with PCR purification kit (Qiagen). The obtained DNA samples were submitted to core facility (UNC) for preparation of multiplexed libraries and deep sequencing. Other datasets include our previously published BRD4 ChIP-seq data (15) and H3K27ac ChIP-seq data from ENCODE in 22Rv1 cells.

ChIP-seq and data analysis

ChIP-seq reads were aligned to the human reference genome (hg19) by the BWA (V0.7.12; default parameters) software (22). After the duplicated reads were removed, MACS2 (v2.1.0; -q 0.1 -m 20 100) (23) was used for calling peaks with input as control. Peaks overlapping (≥1 bp) with the 'blacklist' regions identified by the ENCODE project were also removed. The filtered peaks were then assigned to the annotated (coding and non-coding) genes and defined sequentially as 'promoter' (±2 kb of transcription start site, TSS), within 'gene body', 'distal' (i.e. 'enhancer'; –50 kb to –2 kb of TSS or +2 kb of TSS to +5 kb of transcription ends), or otherwise 'intergenic' using the human RefSeq annotation. The ChIP-seq read densities were calculated and visualized as heatmaps using the program seqMINER (24). The enrichment of motifs was identified by the software HOMER (25) with default parameters. ChIP-seq profiles were visualized in the IntegrativeGenomics Viewer (IGV, Broad Institute).

Gene set enrichment analysis (GSEA)

GSEA was carried out with the downloaded GSEA software (www.broadinstitute.org/gsea) and the Molecular Signatures Database (www.broadinstitute.org/gsea/msigdb/annotate.jsp) as described (15,17,18,26).

Real-time cell metabolic analysis

Cells were cultured in RPMI-1640 medium without phenol red for three days, followed by harvesting, resuspension in the assay medium (Agilent, 103576-100) and plating in the XF24 assay plate (Agilent, 100777-004) at a density of 0.1 million cells per well. The cells were then kept at 37°C without CO_2 for 1 h. Oxygen consumption rate (OCR) was measured using Cell Mito Stress Kit (Agilent, 103015-100) with the following sequential injection of mitochondria inhibitors: 1.5 μM oligomycin, 1 μM Carbonyl cyanide-4-(trifluoromethoxy)phenylhydrazone (FCCP), and then 0.5 uM of Antimycin A and Rotenone. Extracellular acidification rate (ECAR) was measured using Glycolysis Stress Kit (Agilent, 103020-100), with cells metabolically perturbed by sequential injections of 10mM glucose, 1 μM oligomycin and 50 mM 2-deoxyglucose. OCR and ECAR levels were recorded using a Seahorse XF-24 extracellular flux analyzer following manufacturer's instructions (Seahorse Biosciences).

Luciferase reporter assay

Cells were seeded in 24-well plates and co-transfected with plasmids that included the luciferase reporter and the internal control (pRL-CMV Renilla). Luciferase activity was measured 48 h after transfection using the Dual Luciferase Reporter Assay System (Promega). Data were normalized to Renilla luciferase.

BioID

A proximity labeling-based BioID was carried out as described (27,28). In brief, 22Rv1 cells that stably expressed a

Flag-tagged BirA ligase fused in-frame to the N-terminus of YY1 were treated with 50uM of biotin for 24 h, followed by one-hour lysis in the RIPA buffer (10% glycerol, 25 mM Tris–HCl pH 8, 150 mM NaCl, 2 mM EDTA, 0.1% SDS, 1% NP-40 and 0.2% sodium deoxycholate; freshly supplemented with 1× protease inhibitor cocktail, 1 mM PMSF and 250 units of Benzonase) with rotation at 4°C. Cells stably transduced with the BirA ligase only were used as a negative control for BioID. Samples were snap frozen in liquid nitrogen, thawed on ice, and then transferred to Eppendorf tubes. After brief vortex of cell lysate and centrifugation at top speed for 30 min at 4 °C, the cleared supernatant was collected and incubated with Neutravidin beads (Thermo Fisher, #29204) for overnight at 4°C. Beads were washed twice with the RIPA buffer (with no additives), twice with TAP lysis buffer (10% glycerol, 150 mM NaCl, 2 mM EDTA, 0.1% NP-40 and 50 mM HEPES pH 8) and three times with the ABC buffer (50 mM ammonium bicarbonate, pH 8), followed by spin at 400g for 2 min at 4°C. The bead:protein samples were stored in 100 μl of ABC buffer before mass spectrometry-based protein identification.

Mass spectrometry-based protein identification and proteomic data analysis

Proteins bound on beads were eluted by adding 100 μl of 1× Laemmli buffer (Boston Bioproducts) and boiled at 95°C for 5 min. Supernatants were then loaded on a 4–12% Bis–Tris Deep Well gel, resolved by one-dimensional SDS-PAGE and visualized by Coomassie staining. Each SDS-PAGE gel lane was sectioned into 12 segments of equal volume. Each segment was subjected to in-gel trypsin digestion by using the following established protocol. Gel slices were de-stained in 50% methanol (Fisher), 50 mM ammonium bicarbonate (Sigma-Aldrich), followed by reduction in 10 mM Tris(2-carboxyethyl)phosphine (TCEP; Pierce) and alkylation in 50 mM iodoacetamide (Sigma-Aldrich). Gel slices were then dehydrated in acetonitrile (Fisher), followed by addition of 100 ng porcine sequencing grade modified trypsin (Promega) in 50 mM ammonium bicarbonate (Sigma-Aldrich) and incubation at 37°C for 12–16 h. Peptide products were then acidified in 0.1% formic acid (Pierce). Tryptic peptides were separated by reverse phase XSelect CSH C18 2.5 μm resin (Waters) on an in-line 150 × 0.075 mm column using a nanoAcquity UPLC system (Waters). Peptides were eluted using a 30 min gradient from 97:3 to 67:33 buffer A:B ratio (Buffer A = 0.1% formic acid, 0.5% acetonitrile; buffer B = 0.1% formic acid, 99.9% acetonitrile). Eluted peptides were ionized by electrospray (2.15 kV) followed by MS/MS analysis using higher-energy collisional dissociation (HCD) on an Orbitrap Fusion Tribrid mass spectrometer (Thermo) in top-speed data-dependent mode. MS data were acquired using the FTMS analyzer in profile mode at a resolution of 240 000 over a range of 375–1500 m/z. Following HCD activation, MS/MS data were acquired using the ion trap analyzer in centroid mode and normal mass range with precursor mass-dependent normalized collision energy between 28.0 and 31.0. Proteins were identified by searching the UniProtKB database using Mascot (Matrix Science). Scaffold (Proteome Software) was used to verify MS/MS based peptide and protein identifications. Peptide identifications were accepted if they could be established with less than 1.0% false discovery rate by the Scaffold Local FDR algorithm. Protein identifications were accepted if they could be established with less than 1.0% false discovery rate and contained at least two identified peptides. and the counts were normalized to $\log_2$ normalized spectral abundance factor (NSAF) values. Significant interacting proteins were identified by a $\log_2$ fold change >1.

Tumor growth in xenografted animal models

All animal experiments were approved by and performed in accord with the guidelines of the Institutional Animal Care and Use Committee (IACUC) at UNC. One million of 22Rv1 cells were suspended in 100 μl of 1:1 mixture of PBS and Matrigel (BD Biosciences) and subcutaneously (s.c.) injected into dorsal flanks of castrated NOD/SCID/gamma-null (NSG) mice bilaterally (carried out by the Animal Studies Core, UNC Lineberger Comprehensive Cancer Center). Diameter measurements of xenografted tumors were performed twice per week using caliper and the tumor volume calculated.

Statistical analysis

Data are presented as the mean ± SD for three independent experiments unless otherwise noted. Statistical analysis was performed with Student's t-test, except for nonparametric analysis such as gene expression association analysis that employed ANOVA test.

RESULTS

YY1 is significantly upregulated in primary samples of prostate cancer patients

To assess relevance of YY1 in prostate cancer, we first examined the publicly available prostate cancer datasets (29,30) and found the *YY1* mRNA levels significantly elevated in tumors compared to adjacent benign tissues (Figure 1A and B). Next, we performed immunohistochemical (IHC) staining with thirteen paired tumor and normal tissues from prostate cancer patients, and observed the YY1 protein levels to be significantly increased in nuclei of tumors, compared to their respective adjacent benign controls (Figure 1C, D and Supplementary Figure S1; $P = 0.0071$). Immunoblots further verified upregulation of YY1 in prostate tumors, relative to paired benign tissues (Figure 1E). Furthermore, we performed YY1 IHC staining with tissue microarrays that contained a larger panel of benign prostates and samples representing different stages of prostate tumors including adenocarcinoma and CRPC, and found the average level of nuclear YY1 to be significantly higher in CRPC, compared to normal controls ($P = 0.0024$) and adenocarcinomas ($P = 0.0126$), as shown by representative IHC images (Figure 1F) and quantitative analysis (Figure 1G). Overall, these results lend a support for involvement of YY1 in prostate cancer pathogenesis, including CRPC.

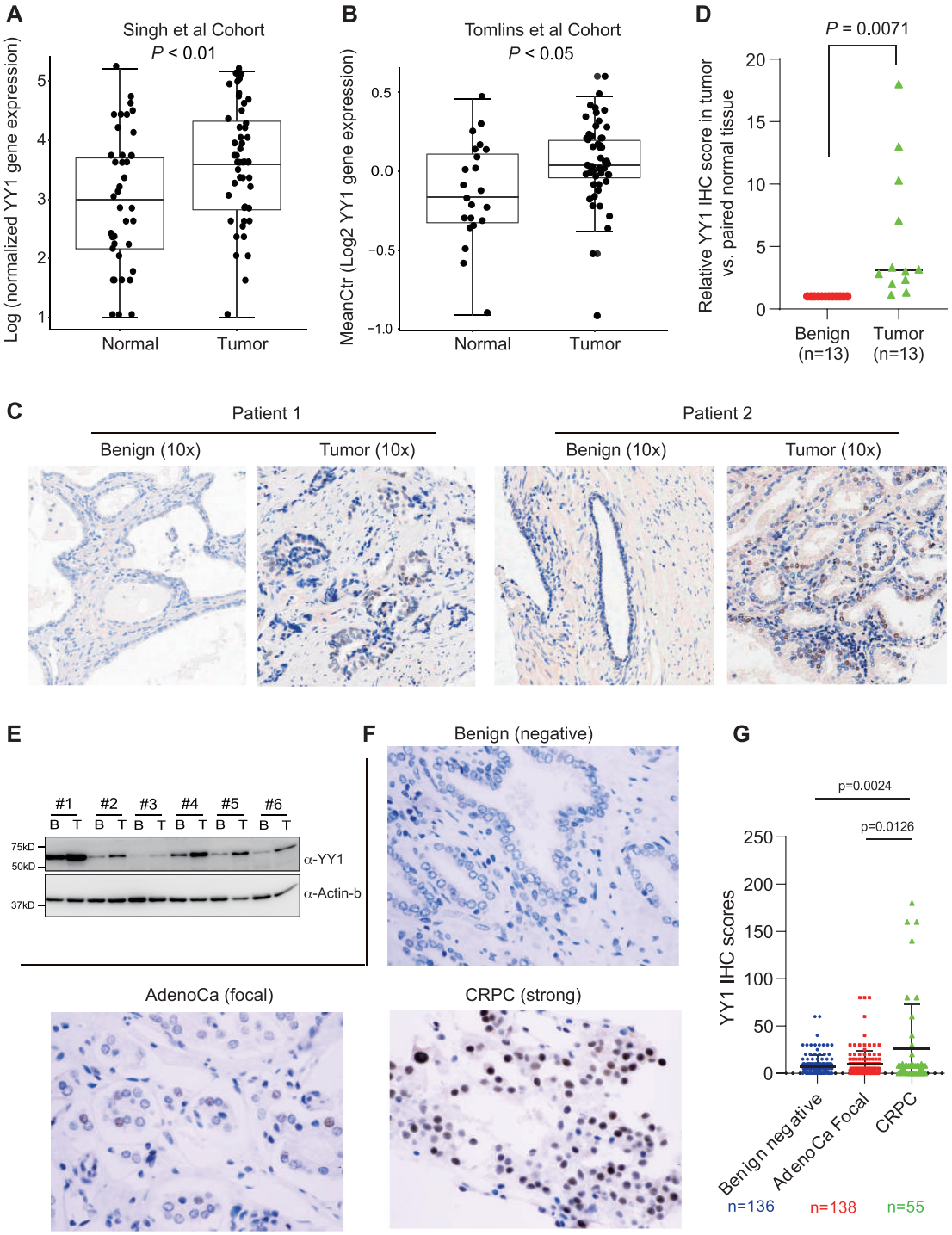

Figure 1. The elevated expression of YY1 is significantly correlated with progression of advanced prostate cancer. (A, B) Boxplots showing overall *YY1* mRNA levels among the prostate cancer patient cohorts reported by Singh *et al.* (29) (**A**) and Tomlins et al (30) (**B**), relative to their respective normal control tissues. (C, D) Representative images (**C**; 10×) and quantification (**D**) of YY1 immunohistochemistry (IHC) staining of thirteen paired prostate tumor and adjacent normal/benign tissues. (**E**) Immunoblotting for YY1 using total protein lysates of the paired normal/benign (**B**) and tumor (T) tissues from prostate cancer patients. β-actin acts as a loading control. (F, G) Representative images (**F**) and quantification (**G**) of YY1 IHC staining by using tissue microarrays (TMA) that contained the samples of benign prostates ($n = 136$), primary prostate adenocarcinoma (AdenoCa; $n = 138$) and CRPC ($n = 55$).

YY1 promotes malignant growth of prostate cancer *in vitro* and *in vivo*

Next, we sought to determine the role for YY1 in prostate tumorigenesis. Using the independent YY1-targeting shRNAs, we performed YY1 knockdown (KD) in two androgen-independent CRPC models, 22Rv1 and C4-2 cells (Figure 2A–F). YY1 KD significantly decreased tumor cell proliferation in liquid culture (Figure 2A, D) and colony formation in soft agar, a surrogate assay of transformation (Figure 2B–C, E–F). Similar phenotypes were observed post-KD of YY1 in LNCaP cells, a prostate cancer model showing androgen dependency (Supplementary Figure S2A and B). Furthermore, reintroduction of YY1 into 22Rv1 cells with endogenous YY1 depleted was able to restore both cell growth and colony formation, thus ruling out potential off-target effects of shRNA (Figure 2G–J). In accordance with the shRNA-mediated YY1 KD, YY1 depletion via two independent sgRNAs through a CRISPR/Cas9 system, or via siRNA, all led to the decreased tumor cell proliferation (Figure 2K, Supplementary Figure S2C and D). In addition, the cell cycle progression and survival of prostate cancer cells also require YY1— upon YY1 depletion, there was an increase in the percentage of cells in the G1-S phase and a concurrent decrease in those in the G2-M phase (Figure 2L, Supplementary Figure S2E); moreover, compared to control, depletion of YY1 led to the enhanced apoptosis as demonstrated by immunoblotting of cleaved caspases (Figure 2M).

To further determine whether YY1 is important for CRPC tumorigenesis *in vivo*, we subcutaneously xenografted 22Rv1 cells, which were stably transduced with control or YY1-targeting shRNA, into NOD/scid/gamma (NSG) mice. 22Rv1 xenografts in the YY1 KD cohort grew in a significantly slower rate, relative to control (Figure 2N and O). Additionally, we validated YY1 KD in tumor xenografts (Figure 2N, insert). Altogether, we conclude that YY1 is crucial for CRPC growth *in vitro* and *in vivo*.

YY1 directly binds to tumor metabolism-related genes, potentiating their transcription

To gain insight into molecular mechanisms underlying the YY1-mediated tumorigenesis in CRPC, we profiled 22Rv1 cell transcriptome by RNA-seq, which revealed differentially expressed genes (DEGs) caused by YY1 KD (Figure 3A and Supplementary Table S1). Gene Set Enrichment Analysis (GSEA) showed that genes down-regulated due to YY1 KD were enriched in pathways related to energy metabolism such as glycolysis (Figure 3B, upper panels), prostate cancer (Figure 3B, bottom/left) and, as expected, the YY1 targets (Figure 3B, bottom/right). Notably, a set of metabolic enzymes involved in glycolysis were downregulated upon YY1 depletion (Figure 3C). To validate this regulatory function of YY1, we additionally performed RNA-seq post-KD of YY1 in another CRPC model (C4-2 cells) and subsequent GO and GSEA analyses revealed similar enrichments of metabolic pathways among genes positively controlled by YY1 (Supplementary Figure S3A-B and Table S2). On the other hand, GSEA analysis of the up-regulated genes following YY1 KD identified the pathways related to apoptosis and cell cycle arrest (Supplementary Figure S3C and D), consistent with our phenotypic studies (Figure 2L and M).

In addition, we identified the genes that were upregulated by YY1 in both CRPC models, hereafter termed 'the YY1 signature genes in CRPC', which included a number of metabolism-associated genes such as *PFKP, ALDOC, OGDHL* and *NDUFA4L2* (Figure 3D, Supplementary Figure S3E and Table S3). Using qRT-PCR, we further confirmed the gene activation effect by YY1 on expression of these metabolic genes in both 22Rv1 and C4-2 cells, with the expression decrease of *PFKP* being most prominent upon YY1 loss relative to control (Figure 3E and F).

We next performed YY1 ChIP-seq to determine its genome-wide binding in 22Rv1 cells, which were either ligand-starved (DHT-) or treated with androgen receptor agonist (DHT+). YY1 binding patterns were highly similar between these two treatment conditions, with 49,066 peaks found to be the common ones (Supplementary Figure S4A). Therefore, we chose to use profiles of vehicle-treated cells for further analysis because this condition resembles CRPC more closely. Genomic localization analysis showed approximately 25% of the YY1 peaks at promoters, ∼36% in gene body, and the rest (∼39%) at putative intergenic and distal enhancers (Figure 3G). As expected, the YY1 motif was most enriched within YY1 peaks (Figure 3H). Also, YY1 peaks were found at almost all of the YY1-upregulated genes defined by RNA-seq, including metabolic genes *PFKP, ALDOC, ENO2* and *NDUFA4L2* (Figure 3I). Moreover, ChIP-seq or ChIP-qPCR of YY1 in two more common prostate cancer models, LNCaP and C4-2 cells, showed the similarly strong enrichments at metabolic genes such as PFKP and ENO2 (Supplementary Figure S4B and C). Taken together, integrated genomic profilings lend a strong support for a direct involvement of YY1 in upregulation of genes related to prostate cancer and cell metabolism.

Bromodomain-containing proteins act as cofactor of YY1

To gain further insight into the mechanism underlying the YY1-mediated tumorigenesis, we examined the YY1 interactome by employing a proximity labeling-based BioID approach (27,28) (Supplementary Figure S4D). Subsequent mass spectrometry-based analysis of YY1-associated factors identified YY2, INO80, TADA2A and BRD2 among the most significantly enriched hits (Figure 4A and B). Previously, INO80 was shown to interact with YY1 (31), suggesting fidelity of our approach. YY1-binding motif was reported to be enriched in the promoters of BRD2-bound genes in a non-small cell lung cancer cell line H23 (32), indicative of a putative association; however, such a connection between YY1 and BRD2 has not been further explored. We found that BRD2 depletion significantly inhibited 22Rv1 cell proliferation (Figure 4C). Co-immunoprecipitation (CoIP) further verified the interaction of YY1 with BRD2 and a BRD2-related protein, BRD4, in 22Rv1 cells (Figure 4D) and C4-2 cells (Supplementary Figure S4E). Bromodomain-containing proteins BRD4 and BRD2 can bind to acetylation sites within the histones (33) (such as H4 and H3 acetylation) or DNA-binding

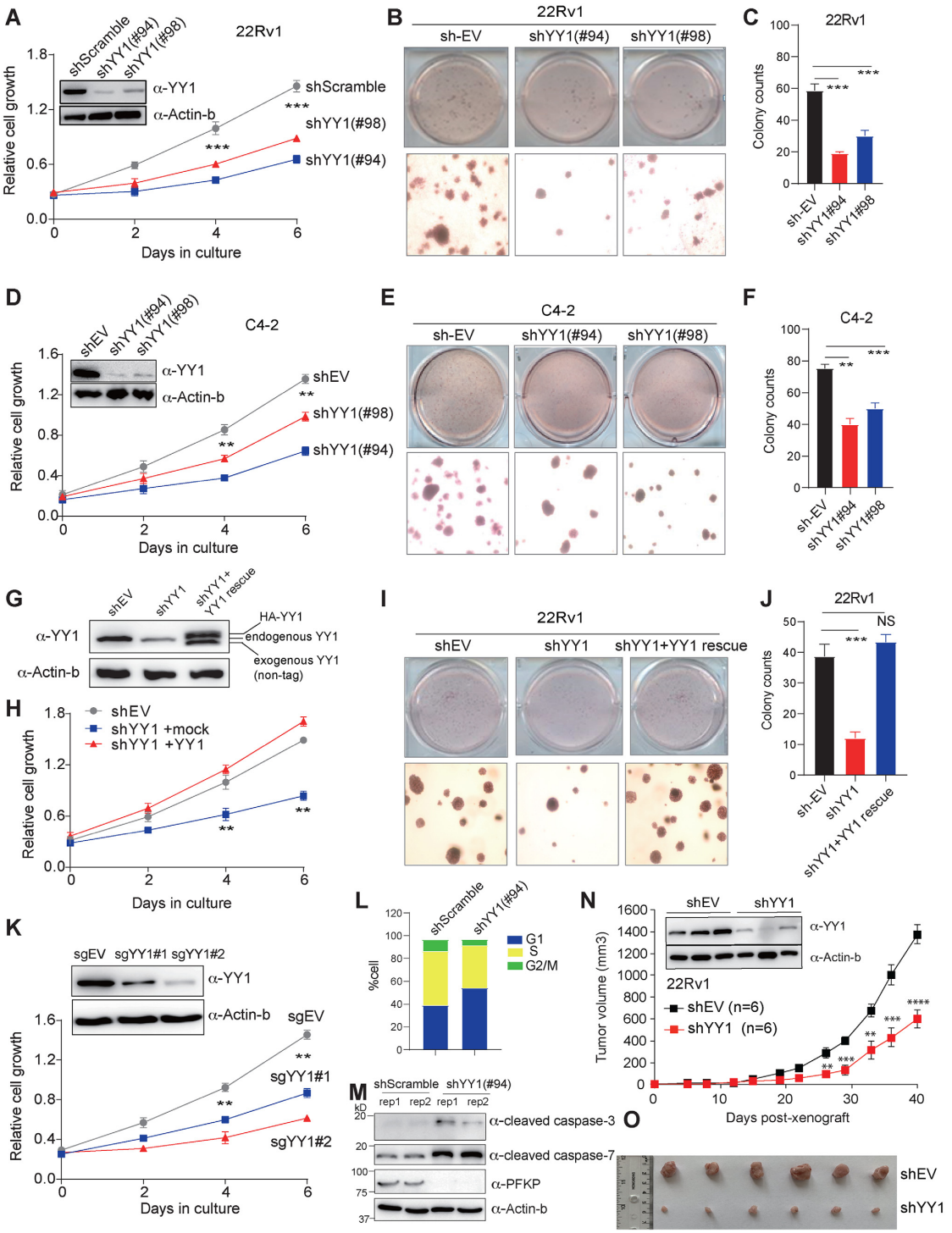

Figure 2. YY1 is required for malignant growth of prostate tumor cells *in vitro* and *in vivo*. (**A–F**) Immunoblotting for YY1 and measurement of cell proliferation (A and D), as well as assessment of the soft agar-based growth of 22Rv1 (B, C) or C4-2 (E, F) cells (with representative images shown in B and E), after shRNA-mediated knockdown (KD) of YY1 (sh#94 or sh#98), relative to transduction of either scramble shRNA or empty vector (shEV). $^{**}P < 0.01$; $^{***}P < 0.001$. (**G–J**) Immunoblotting for YY1 (using antibody against endogenous YY1; G), measurement of cell proliferation (H), and assessment of the soft agar-based growth (I–J; with representative images shown in I) after rescue of YY1 expression, relative to mock, in the 22Rv1 cells with endogenous YY1 knocked down (sh#94, which targets the 3'-UTR of YY1). Please note that an HA-tagged YY1 rescue construct used in the study produces two species of YY1, either with tag or without (see the labels in G). $^{**}P < 0.01$; $^{***}P < 0.001$. (**K**) Immunoblotting of YY1 and measurement of 22Rv1 cell proliferation after the CRISPR/cas9 mediated depletion of YY1, relative to mock treatment (sgEV). $^{**}P < 0.01$. (**L**, **M**) Quantification of cell cycle phases (L) and immunoblotting of the indicated apoptotic markers (M; $n = 2$ replicated samples) using the 22Rv1 cells post-KD of YY1, compared to mock-treated. (**N**, **O**) Summary of xenografted tumor sizes (N; mean ± SD in y-axis) after subcutaneous transplantation of 22Rv1 cells, which were stably transduced with shEV (black) or shYY1 (red), into castrated NSG mice ($n = 6$ per group). $^{**}P < 0.005$, $^{***}P < 0.0005$, $^{****}P < 0.0001$. Immunoblotting of YY1 and images of tumor xenografts excised at the study endpoint are shown in N (insert) and O, respectively.

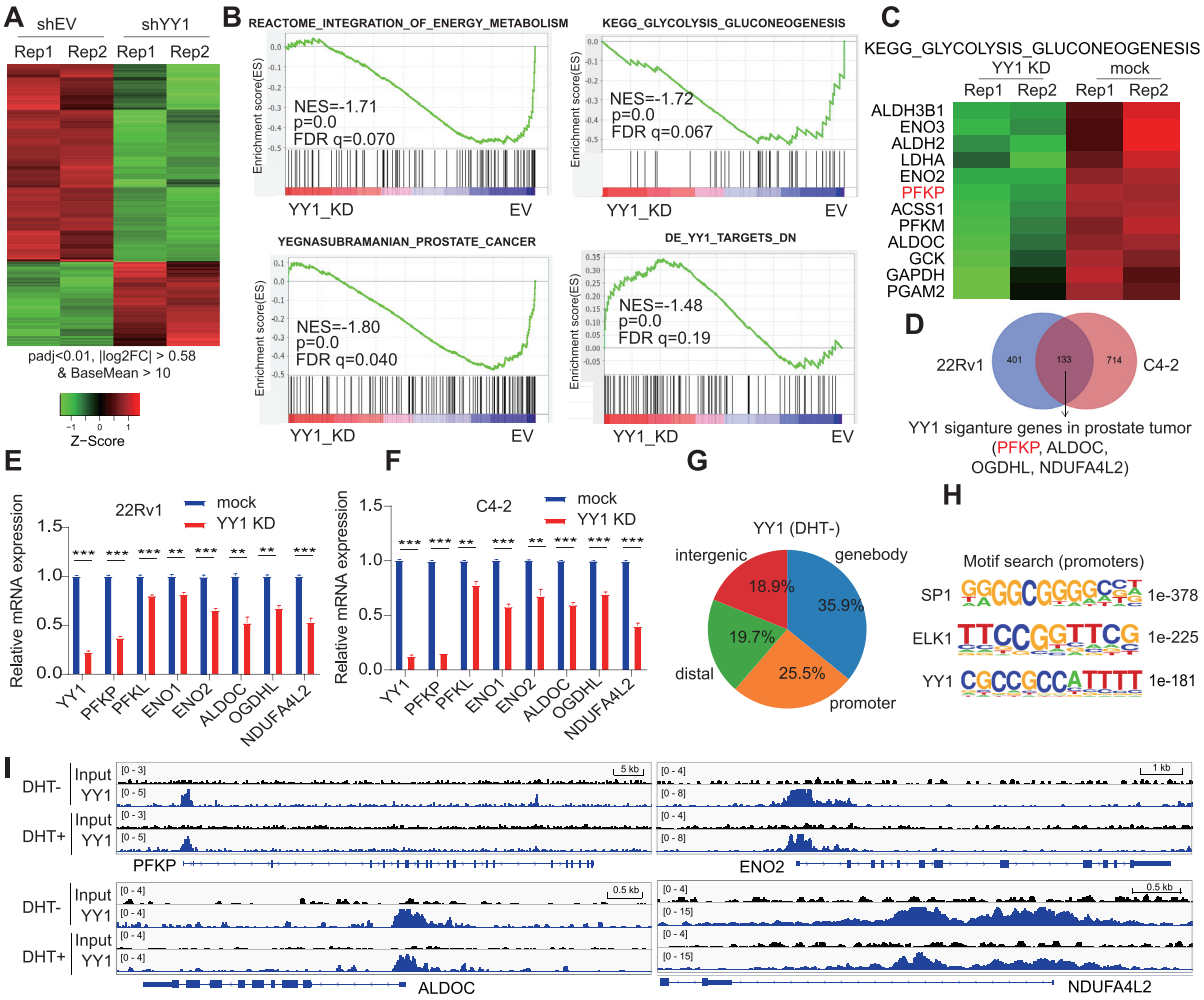

Figure 3. YY1 directly binds to and activates the metabolic genes in prostate tumor. (**A**) Heatmap showing expression of the differentially expressed genes (DEGs) identified by RNA-seq in 22Rv1 cells post-KD of YY1, relative to mock-treated ($n = 2$ two biological replicates per group). Threshold of DEG is set at the adjusted DESeq *P* value (padj) less than 0.01 and |fold-change (FC)| over 1.5 for transcripts with mean tag counts of at least 10. (**B**) GSEA shows that, relative to mock, YY1 depletion in 22Rv1 cells is correlated with downregulation of the indicated genes related to energy metabolism, glycolysis or prostate cancer, and as expected, correlated with the indicated YY1-repressed genes. (**C**) Heatmap showing expression of the indicated glycolysis-related genes in 22Rv1 cells after YY1 KD, relative to mock. (**D**) Venn diagram showing overlap between the YY1-upregulated genes identified by RNA-seq in 22Rv1 (left) and C4-2 (right) cells. Threshold of DEG is set at the adjusted DESeq *P* value (*P*adj) less than 0.01 and |FC| over 1.5 for transcripts with mean tag counts of at least 10. (E, F) RT-qPCR of YY1 and the indicated metabolic gene using 22Rv1 (**E**) and C4-2 (**F**) cells post-KD of YY1, compared to mock. Y-axis shows the averaged FC in gene expression after normalization of RT-qPCR signals to beta-Actin and then to mock-treated ($n = 3$ independent experiments). ** $P < 0.01$, *** $P < 0.001$. (**G**) Pie chart showing genomic distribution of the called YY1 ChIP-seq peaks in 22Rv1 cells. (**H**) Motif search analysis revealing the most enriched motifs at the called YY1 ChIP-seq peaks. (**I**) IGV views of chromatin input and the YY1 ChIP-seq peaks (depth normalized) at the indicated metabolic gene in 22Rv1 cells, which were first ligand-starved followed by treatment with vehicle (DHT–) or dihydrotestosterone (DHT+).

factors to mediate transcriptional activation (34), which is achieved at least partially through recruiting the BRD4-pTEFb complex to boost the release of RNA Pol-II into a productive elongation phase (35–38). We also found the bromodomains of BRD4 to be required for efficient interaction with YY1 (Figure 4E). In agreement, the bromodomain inhibitor JQ1 significantly decreased the interaction between YY1 and BRD4 (Figure 4F). Interestingly, YY1 was shown to be acetylated at a Lys-rich region (amino acids 170–200) (39) (Figure 4G). Relative to WT, the lysine-to-arginine mutations of this Lys-rich region in YY1 significantly decreased the YY1 interaction with BRD4 (Figure 4H), further supporting that lysine acetylation within YY1 and the BRD4 bromodomains mediate the interaction between the two. In addition, CoIP further showed YY1 interaction with TADA2A (Figure 4I), an adaptor and subunit of ATAC/GCN5 histone acetyltransferase complex (40,41), which suggests that YY1 may recruit/assemble a complex containing BRD2/4 (acetylation 'reader') and GCN5/ATAC complex (acetylation 'writer'), thereby forming a feed-forward loop for gene activation. In support, we found a striking overlap of YY1 with BRD4 and H3K27ac (Figure 4J). Of note, about 90% of H3K27ac ChIP-seq peaks are co-localized with those of YY1 in 22Rv1 cells

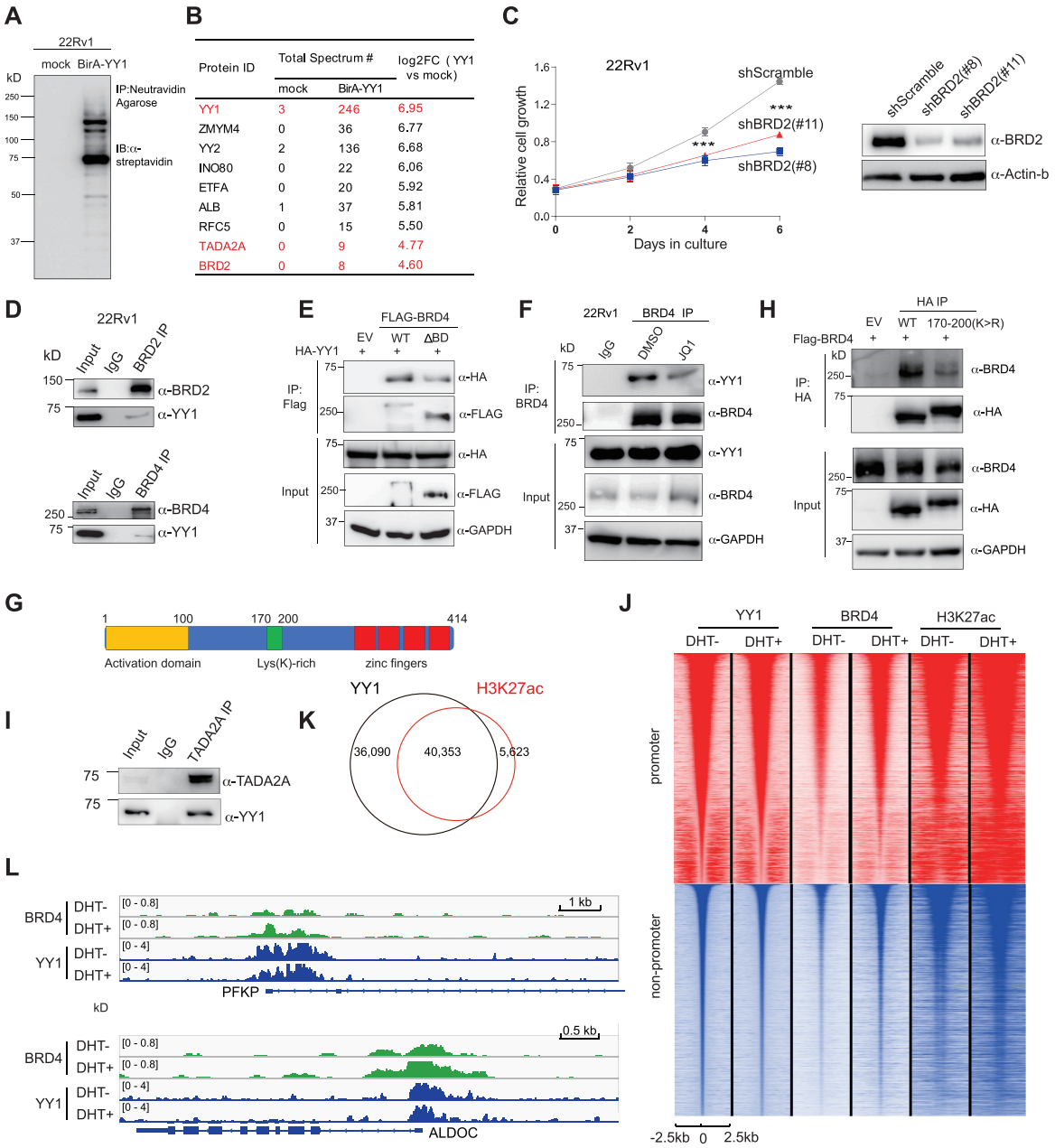

Figure 4. Bromodomain-containing proteins serve as co-activator of YY1, potentiating the expression of metabolic genes in prostate cancer. (**A**) Immunoblot of the biotinylated proteins (probed with streptavidin-HRP conjugate) after treatment of 22Rv1 cells, which were stably transduced with a biotin ligase only (mock; lane 1) or BirA-YY1 fusion (lane 2), with 50 uM of biotin for 24 h. (**B**) Summary of the top hits identified by BioID followed by mass spectrometry in the indicated 22Rv1 cells. (**C**) Measurement of 22Rv1 cell proliferation (left) and BRD2 immunoblotting (right) after KD of BRD2 (sh#8 or sh#11), relative to transduction of scramble shRNA (shScramble). *** $P < 0.001$. (**D**) Co-immunoprecipitation (CoIP) for interaction between endogenous YY1 and bromodomain-containing proteins, BRD2 (top) and BRD4 (bottom), in 22Rv1 cells. (**E**) CoIP for interaction between the exogenously expressed BRD4 (Flag-tagged), either WT or with deletion of tandem bromodomain (BD) domains (ΔBD), and HA-tagged YY1 in 293 cells. (**F**) CoIP for YY1:BRD4 interaction in 22Rv1 cells after treatment of DMSO or 500 nM of JQ1 for 8 h. (**G**) Diagram showing the domain architecture of YY1. (**H**) CoIP for interaction between the exogenously expressed Flag-BRD4 and HA-YY1, either WT or a mutant form with six lysines in the Lys (K)-rich region mutated to arginines (170–200[K→R]; also refer to panel **G**), in 293 cells. (**I**) CoIP for interaction of endogenous YY1 with ADA2A, a subunit of the GCN5/ATAC histone acetyltransferase complex, in 22Rv1 cells. (**J**) Heatmap of the YY1, BRD4 and H3K27ac ChIP-seq read densities at the promoter (top) and non-promoter (bottom) YY1 peaks in either ligand-stripped (DHT–) or DHT-treated (DHT+) 22Rv1 cells. The YY1 peaks from two cell conditions were combined, sorted, and used to compute ChIP-seq read densities within 5 kb of the YY1 peak centers. (**K**) Venn diagram showing overlap between the called YY1 and H3K27ac ChIP-seq peaks identified from ligand-stripped 22Rv1 cells. (**L**) IGV views of the YY1 and BRD4 ChIP-seq profiles at the indicated glycolytic gene in vehicle- (DHT–) or DHT-treated (DHT+) 22Rv1 cells.

(Figure 4K). Likewise, BRD4 bindings are significant at the YY1 promoter peaks, nearly as strong as YY1, and at most of the YY1 non-promoter peaks (Figure 4J), as exemplified by those at metabolic genes PFKP and ALDOC (Figure 4L and Supplementary Figure S4F).

YY1 is required for efficient recruitment of bromodomain-containing proteins onto target genes, and bromodomain inhibition suppresses the YY1-mediated gene activation and tumor cell growth

Next, we aimed to assess the causal relationship regarding the chromatin recruitment of YY1 and BRD2/4. We found that YY1 depletion significantly decreased the BRD2/4 binding to the tested metabolic gene promoters (Figure 5A and B); likewise, H3K27ac at these regions was strongly attenuated (Figure 5C). In contrast, bromodomain inhibition by JQ1 treatment did not interfere with YY1 binding to the same regions (Figure 5D). These results suggest that YY1 acts to recruit the BET family of bromodomain proteins to chromatin targets, but not vice versa. Treating 22Rv1 cells with JQ1 dramatically decreased overall expression of the YY1 signature genes including metabolism-related transcripts (Figure 5E and Supplementary Figure S5A). RT-qPCR further validated inhibitory effects by JQ1 on YY1 target genes such as PFKP, ENO1 and ENO2 (Figure 5F). Additionally, YY1 overexpression enhanced proliferation and soft agar colony formation of 22Rv1 cells, which were counteracted by JQ1 treatment (Supplementary Figure S5B and C). In summary, YY1 associates with bromodomain-containing coactivators in prostate cancer, mediating activation of the downstream oncogenic gene-expression program.

PFKP is a direct target of YY1 in prostate cancer

Volcano plots using RNA-seq profiles of 22Rv1 (Figure 6A) and C4-2 cells (Figure 6B) both pointed to PFKP, one of the most altered transcripts upon YY1 depletion. Examination across the transcriptomic datasets of patient samples (30,42,43) showed that the *PFKP* expression is not only correlated with that of YY1 (Figure 6C) but also significantly higher among the prostate tumors, compared to benign tissues (Figure 6D and E), suggesting its potential role in prostate cancer progression. As well, the protein level of PFKP was significantly decreased after YY1 ablation, relative to control, in two tested CRPC cells (Figure 6F). Phosphorylation of YY1 at serine 365 within the zinc figure (Figure 4G) was previously reported to interfere with the DNA binding by YY1 (44). We found that rescue of YY1 loss by an exogenous wildtype YY1 ($YY1^{WT}$) restored cellular level of PFKP (Figure 6G, middle vs left lanes), an effect not seen with $YY1^{S365D}$ (Figure 6G, right vs middle lane). This indicates that PFKP induction by YY1 is DNA-binding-dependent, in agreement with our ChIP-seq data showing YY1 binding to the PFKP promoter (Figure 6H). Indeed, $YY1^{WT}$, but not the $YY1^{S365D}$ mutant, increased transcription from a luciferase-based reporter that carries either a 2 kb-long (Figure 6I) or 575bp-long sequence upstream of PFKP's transcriptional start site (TSS; Figure 6J; based on ChIP-seq data shown in Figure 6H). There are four YY1-binding motifs, CCAT, within the YY1 peak at the PFKP promoter (Supplementary Figure S6). Systematic mutagenesis of these YY1-binding motifs (Figure 6K; CCAT mutated to CGGT) revealed the first and third motifs, and not the second and fourth ones, to be essential for the PFKP promoter-driven transactivation activity in both 22Rv1 and C4-2 cells (Figure 6L and M). Additionally, in contrast to the single motif mutation, compound mutation of the first and third YY1 motifs further decreased the activity of the PFKP promoter (Figure 6L and M; last panels). Thus, YY1 activates PFKP through directly binding its promoter, particularly through the first and third conserved CCAT motifs.

YY1 potentiates prostate tumor cell glycolysis partly via PFKP

Given that PFKP is a rate-limiting enzyme of glycolysis (13), we next assessed whether YY1 regulates cancer cell metabolism by real-time measurements of basal extracellular acidification rate (ECAR), a key marker of glycolysis, and observed it to be dramatically decreased after YY1 loss, relative to mock, in three independent prostate tumor models—22Rv1, C4-2 and LNCaP cells (Figure 7A, B, Supplementary Figure S7A). Relative to control, YY1 depletion also led to the significantly reduced levels of basal oxygen consumption rate (OCR) and maximal respiratory capacity (Supplementary Figure S7B-C). The N-terminal acidic transactivation domain of YY1 (amino acids 1–100; Figure 4G) was reported to be essential for its gene activation function (45,46). Overexpression of $YY1^{WT}$, but not a mutant with deletion of this transactivation domain (Figure 7C, supplementary Figure S7D), enhanced glycolysis of 22Rv1 and C4-2 cells (Figure 7D and E), which is in agreement with the metabolic defects seen upon YY1 depletion. Requirement of the YY1 transactivation domain for promoting tumor cell glycolysis is also in line with YY1's role for transactivation of glycolysis-related genes revealed by RNA-seq.

Given that BET bromodomain proteins are YY1 cofactors and that JQ1 treatment inhibited the YY1-related metabolic gene activation (Figure 5E and F), we further assessed the role of bromodomain proteins in glycolysis. Indeed, BRD2 depletion significantly reduced glycolysis of 22Rv1 cells (Figure 7F). Likewise, JQ1 treatment suppressed the increase of glycolysis caused by YY1 overexpression (Figure 7G, red versus green). These data supported a requirement of bromodomain proteins for YY1-mediated enhancement of glycolysis.

We also aimed to delineate the YY1 target(s) responsible for enhanced glycolysis or the Warburg effect. Among the common YY1-upregulated transcripts included *PFKP, ALDOC* and *ENO2* (Figure 3C). While the ectopic expression of ENO2 or ALDOC failed to significantly rescue the glycolysis defects caused by YY1 depletion (Supplementary Figure S7E–H), PFKP largely reversed the reduction of glycolysis (Figure 7H and I). In agreement, KD of PFKP by independent hairpins significantly diminished the rate of glycolysis in both 22Rv1 and C4-2 cells (Figure 7J and K); as well, depletion of PFKP almost completely abolished the effect of YY1 overexpression on glycolysis (Figure 7L and M). Thus, YY1 plays an essential role in potentiating glycol-

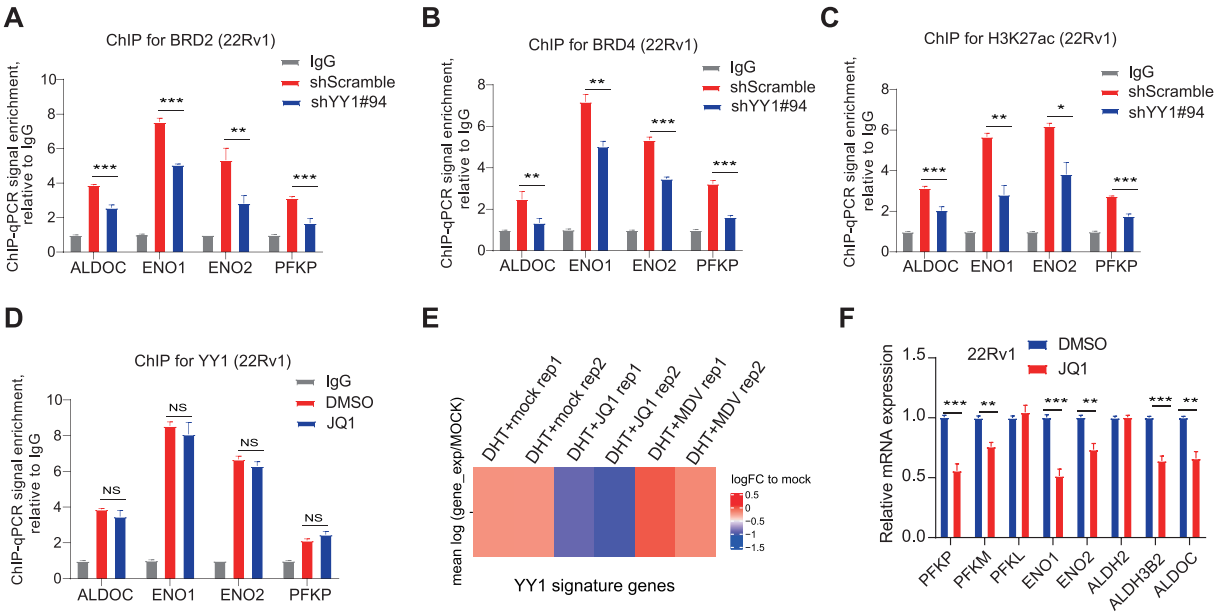

Figure 5. YY1 is required for efficient recruitment of the BET bromodomain-containing proteins to downstream targets in prostate cancer cells. (**A-C**) ChIP-qPCR for BRD2 (**A**), BRD4 (**B**) and H3K27ac (**C**) at the indicated glycolytic gene promotor in 22Rv1 cells after YY1 KD (sh#94), relative to mock. Y-axis shows the averaged fold-change in ChIP-qPCR signals after normalization to those of input and then to IgG control ($n = 3$ independent experiments). ** $P < 0.01$, *** $P < 0.001$. (**D**) ChIP-qPCR of YY1 binding to the indicated glycolytic gene promotor in 22Rv1 cells post-treatment with DMSO or 500nM of JQ1 for 8 h. Y-axis shows the averaged fold-change in ChIP-qPCR signals after normalization to those of input and then to IgG control ($n = 3$ independent experiments). NS, not significant. (**E**) Heatmap showing overall change in expression of the YY1 gene signature (defined in Figure 3D) in 22Rv1 cells treated with either DHT alone, DHT plus JQ1, or DHT plus the AR antagonist MDV3100 (MDV). Color bar, mean of log(Fold-change). (**F**) RT-qPCR of the indicated metabolic gene in 22Rv1 cells after an eight-hour treatment with either DMSO or 500 nM of JQ1. Y-axis shows the averaged fold-change in RT-qPCR signals after normalization first to those of beta-Actin and then to mock-treated ($n = 3$ independent experiments). ** $P < 0.01$, *** $P < 0.001$.

ysis in prostate tumor, an event that relies at least partially on upregulation of *PFKP*.

PFKP is critically involved in prostate tumorigenesis *in vitro* and *in vivo*

PFKP was reported to be involved in oncogenesis such as lung cancer development (47). However, the role of PFKP in prostate tumorigenesis was previously unexplored. Following depletion of PFKP in 22Rv1 and C4-2 cells, we observed the significantly decreased levels of proliferation *in vitro* (Figure 8A and B and Supplementary Figure S8A) and soft agar-based colony formation (Figure 8C-D), relative to mock. As well, both the cell cycle progression (Figure 8E and Supplementary Figure S8B) and survival of prostate cancer cells (Figure 8F) were significantly affected upon PFKP depletion. Importantly, overexpression of PFKP in the YY1-depleted 22Rv1 or C4-2 cells partially but significantly rescued the ameliorated proliferation phenotype caused by YY1 loss (Figure 8G and H). In the 22Rv1 cell xenografted mouse model, PFKP loss also dramatically decreased tumor growth (Figure 8I–K). Therefore, PFKP, a downstream onco-target of YY1, is essential for prostate cancer progression (see model Figure 8L).

DISCUSSION

In this report, we show that YY1 is significantly overexpressed during progression of prostate cancer and plays a pivotal role in prostate oncogenesis across independent models, such as AR-dependent and CRPC cell lines and xenografted animal models. Furthermore, our YY1 cistrome studies demonstrate that YY1 directly binds to and mediates transactivation of metabolic genes including PFKP. Both YY1 and PFKP are paramount for potentiating tumor cell metabolism including glycolysis and mitochondria respiration. Of note, YY1 was reported to mediate tumorigenesis in a range of cancers such as breast tumor, lung cancer and melanoma (5,7,48–51), and recently, it has been shown that YY1 also regulates cell metabolism in different biological contexts including cancer, muscle regeneration and neural crest development (52–58). Likewise, PKFP was known to sustain metabolism in lung and breast cancers (47,59–61), indicating that our reported YY1-PFKP axis may play a more generalized role in malignancies. Please note that, in addition to PFKP, YY1 is most likely to regulate other oncogenesis-related targets in prostate tumor, which merits further investigation.

Via mass spectrometry-based interactome study and subsequent genomic profiling analyses, we additionally identified the BET bromodomain-containing family proteins (BRD2 and BRD4) as functional partners of YY1, providing a mechanistic explanation for the YY1-induced transcriptional potentiation of downstream onco-targets seen in advanced CRPC. In consistence, ~90% of H3K27ac sites are co-bound by YY1 in 22Rv1 cells. We thus favor a view that YY1 likely acts as a master regulator of prostate oncogenesis by sustaining tumor cell metabolism

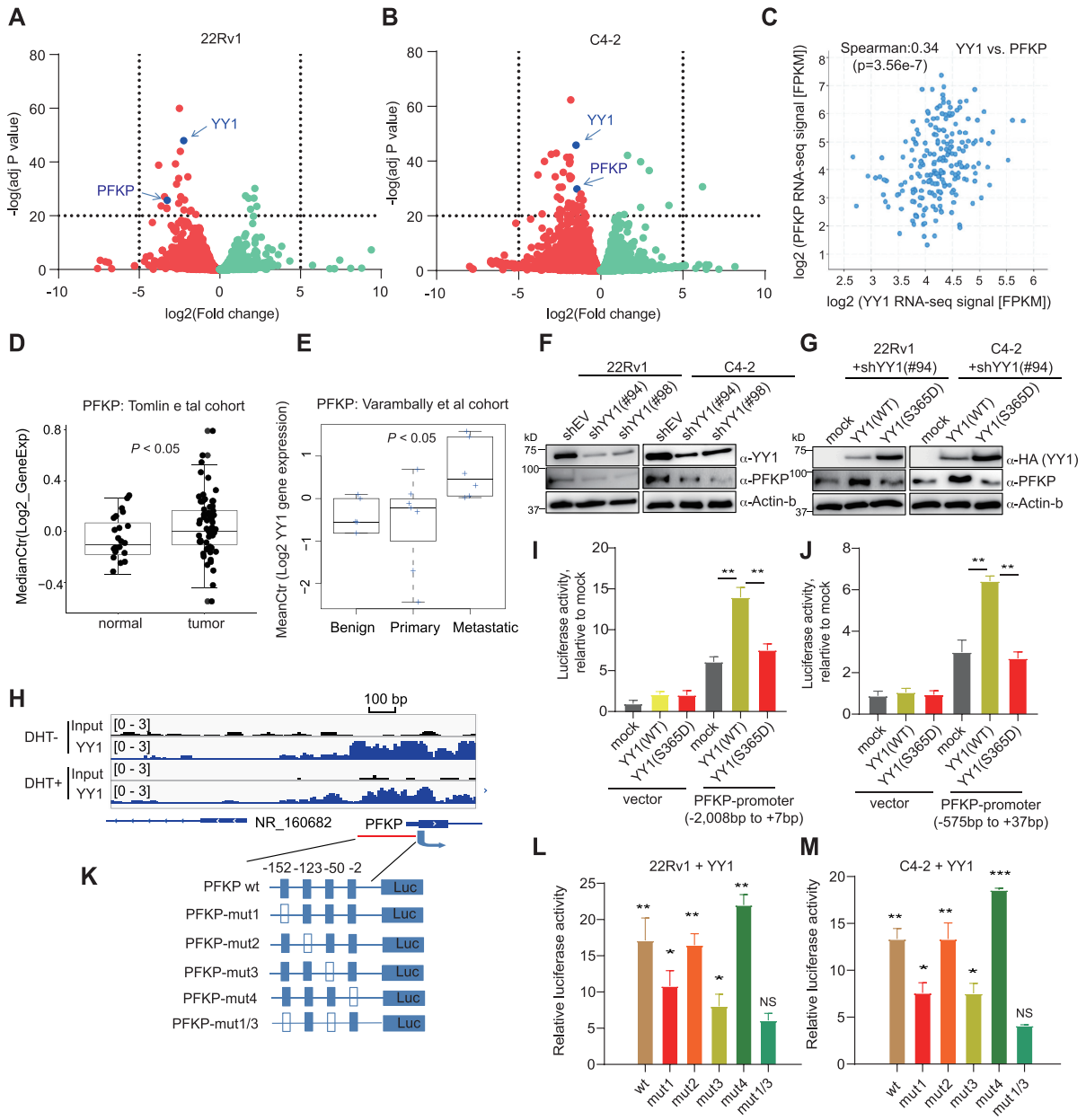

Figure 6. PFKP is a direct onco-target of YY1 in prostate cancer. (A, B) Volcano plots of the RNA-seq profiles highlight *PFKP* among the most altered transcripts upon YY1 depletion in 22Rv1 (**A**) and C4-2 (**B**) cells. (**C**) Correlation between the expression levels of PFKP and YY1 among prostate cancer patients using the StandUp2Cancer (SU2C) dataset (43). (D, E) Box plots showing the *PFKP* expression levels among patient samples from the indicated cohort reported by Tomlins et al (30) (**D**) or Varambally et al (42) (**E**). (**F**) Immunoblotting of endogenous YY1 and PFKP post-KD of YY1, relative to mock, in 22Rv1 (left) and C4-2 (right) cells. (**G**) Immunoblotting of exogenous YY1 (using HA antibody) and endogenous PFKP post-transduction of HA-tagged $YY1^{WT}$ or $YY1^{S365D}$ into 22Rv1 (left) or C4-2 (right) cells with stable YY1 KD (by shYY1#94, which targets 3'-UTR of YY1). (**H**) IGV views of the YY1 ChIP-seq profile at the proximal promoter of *PFKP*. (I, J) Relative transcription activities from a luciferase reporter that carries the *PFKP* promoter (right panel), either –2008 to +7 (**I**) or –575 to +37 bp (**J**) from transcription start site, after its co-transduction with HA-tagged $YY1^{WT}$ or $YY1^{S365D}$ into 22Rv1 cells. Left panels show the reporter results using the cells transduced with the empty luciferase reporter. Y-axis shows the averaged fold-change in the reporter signals after normalization to those of internal luciferase control and then to mock samples (the first sample); $n = 3$ independent experiments; ** $P < 0.01$. (**K**) Scheme shows the used mutation (mut) of putative YY1-binding sites within the *PFKP* promoter. Empty box denotes the mutated YY1-binding site. (L, M) Luciferase activity from a PFKP promoter reporter, which carries either WT or the indicated mutation of YY1-binding sites (refer to K), after its co-transduction with WT YY1 cDNA into 22Rv1 (**L**) or C4-2 cells (**M**). Y-axis shows the averaged fold-change in the reporter signals after normalization to those of internal luciferase controls and then to empty vector-transfected cells (n = 3 independent experiments). * $P < 0.05$; ** $P < 0.01$; *** $P < 0.001$; NS, not significant.

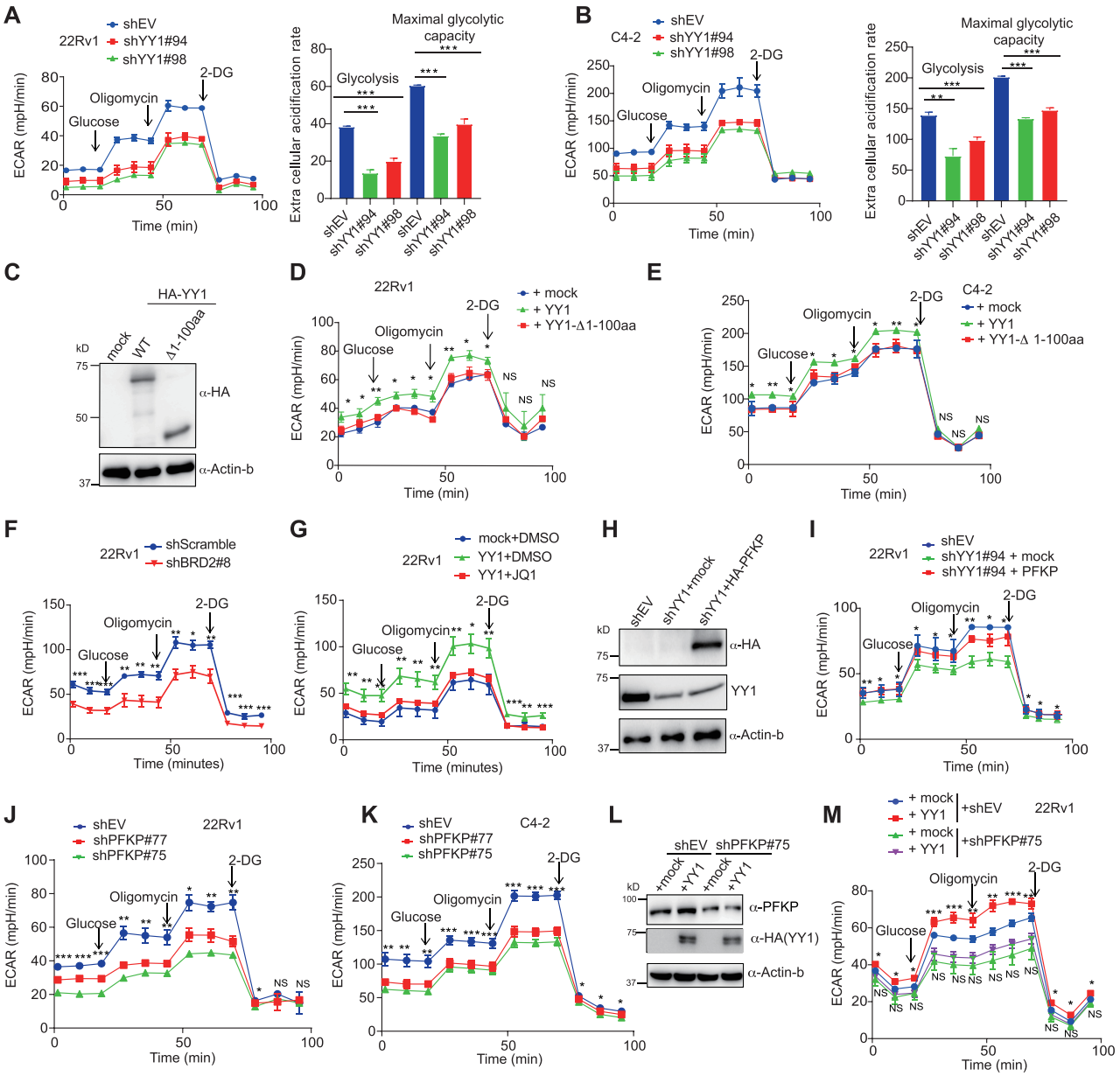

Figure 7. YY1 potentiates prostate tumor cell glycolysis partly via PFKP. (A, B) Measurement of extra cellular acidification rate (ECAR) in 22Rv1 (**A**) or C4-2 cells (**B**) after YY1 KD, compared to mock (shEV). The scheme showing the injection of compounds during the assays is presented in the left panel. Data quantifications are shown in the right panel as mean ± SEM. ** $P < 0.01$, *** $P < 0.001$. (C–E) Immunoblotting for exogenous HA-YY1 (**C**; anti-HA immunoblot), as well as ECAR measurement using the 22Rv1 (**D**) or C4-2 (**E**) cells post-transduction of the indicated HA-YY1, either WT or with its N-terminal transactivation domain deleted (Δ1–100aa). *$P < 0.05$; **$P < 0.01$; NS, not significant. (**F**) ECAR measurement using the 22Rv1 cells post-KD of BRD2 (sh#8), compared to scramble control. * $P< 0.05$; ** $P < 0.01$; *** $P < 0.001$. (**G**) ECAR measurement using 22Rv1 cells, which were transduced with empty vector (mock) or WT YY1, followed by cell treatment with either DMSO or 500nM of JQ1 for 8 h. * $P < 0.05$; ** $P < 0.01$; *** $P < 0.001$. (H, I) Immunoblotting for endogenous YY1 and exogenous HA-PFKP (**H**) and ECAR measurement (**I**) after transduction of empty vector (mock) or HA-PFKP (**H**, lane 3 versus 2), into the YY1-depleted 22Rv1 cells (lanes 2–3). The shEV-transduced cells (lane 1) serve as control. * $P < 0.05$; ** $P < 0.01$; NS, not significant. (J, K) ECAR measurement using the 22Rv1 (**J**) or C4-2 (**K**) cells post-KD of PFKP (sh#75 or sh#77), compared to mock (shEV). * $P < 0.05$; ** $P < 0.01$; *** $P < 0.001$. (L, M) Immunoblotting for endogenous PFKP and exogenous HA-YY1 (**L**) and ECAR measurements (**M**) after transduction of vector (mock; L, lanes 1 and 3) or HA-tagged YY1 (L, lanes 2 and 4) into 22Rv1 cells with stable expression of either shEV (lanes 1–2) or YY1-targeting shRNA (lanes 3–4). * $P < 0.05$; ** $P < 0.01$; NS, not significant.

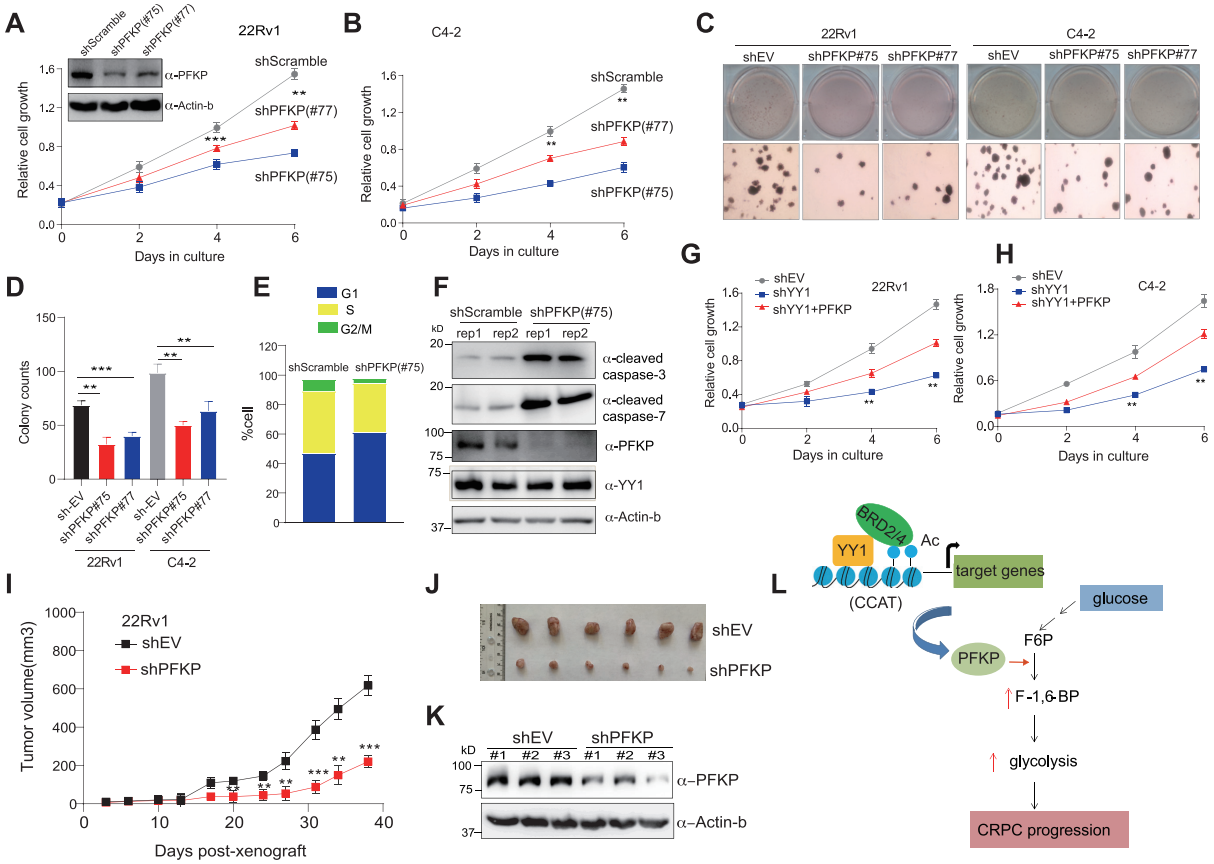

Figure 8. PFKP is critically involved in prostate tumorigenesis *in vitro* and *in vivo*. (A, B) Assays for 22Rv1 (**A**; insert, PFKP blotting) or C4-2 (**B**) cell proliferation after PFKP depletion (sh#75 or sh#77), compared to transduction of a scramble shRNA (shScramble). $*P < 0.05$; $**P < 0.01$; $***P < 0.001$. (C, D) Soft agar-based growth of 22Rv1 (**C**; left) or C4-2 cells (**C**; right) and quantification of colony number (**D**) after PFKP depletion, compared to mock. $*P < 0.05$; $**P < 0.01$; $***P < 0.001$. (E, F) Quantitation of cell cycle phases (**E**) and immunoblotting of the indicated apoptotic markers (**F**; $n = 2$ replicated samples) after PFKP depletion, compared to mock, in 22Rv1 cells. (G, H) Assays for cell proliferation after transduction of empty vector (blue) or an exogenous PFKP (red) into the YY1-depleted 22Rv1 (**G**) or C4-2 cells (**H**); cells without YY1 depletion were used as control (shEV; gray). ** $P < 0.01$. (**I–K**) Summary of xenografted tumor sizes (**I**) after subcutaneous transplantation of 22Rv1 cells, which were stably transduced with shEV (black) or shPFKP (red), into castrated NSG mice ($n = 6$ per group). ** $P < 0.005$, *** $P < 0.0005$. The images of tumor xenografts isolated at the end of study and immunoblotting of PFKP in these samples are shown in J and K, respectively. (**L**) Model illustrating the requirement of YY1 and bromodomain-containing coactivators for potentiation of the expression of genes related to energy metabolism in advanced prostate tumor.

and energy production during progression into the advanced disease, CRPC. Additionally, our study shed light on potential strategies. For example, the bromodomain-containing proteins and metabolic pathways activated by YY1 are both druggable by the existing small-molecule inhibitors, which merits additional study. Altogether, our findings unveil a previously unexplored axis involving YY1 and bromodomain-containing coactivators, which act on downstream metabolic genes (such as PKFP and, potentially, other onco-targets) to sustain aggressive phenotypes of prostate cancer.

The cellular functions of YY1 are rather complex (5,7). We show that, in prostate cancer, YY1 and its bromodomain-containing coactivators occupy a large majority of H3K27ac-demarcated cis-elements, potentiating target gene transactivation. In prostate cancer cells, we additionally identified TADA2A, a subunit of the ATAC complex, which is consistent with the reported YY1 interaction to p300 and GCN5, another set of HAT/coactivators (5,39). By gene depletion experiment, we also show that YY1 is required for efficient recruitment of bromodomain-containing coactivators to its targets, but not vice versa. It is thus likely that YY1 is able to assemble coactivator complexes that consist of both HAT (acetylation 'writers') and bromodomain proteins (acetylation 'readers'), thereby establishing a feedforward circuitry during pathogenesis. As well, a lysine-rich region within YY1 was reported to be modified by the antagonizing HDACs and HATs (such as p300 or GCN5) (39). Here, we observed that the acetylation-incompetent mutations of YY1 (harboring Lys-to-Arg substitutions within the Lys-rich region) largely abolished its interaction with BRD4, an effect also seen with treatment of bromodomain inhibitors. These data lend a strong support that lysine acetylation within YY1 directs BRD4:YY1 interaction. In contrast to involvement in coactivator complexes, YY1 was also shown to interact with a set of gene-repressive factors such as HDACs (5,39) and Polycomb Repressive Complex (PRC) (62–66). It is intriguing to propose that YY1 can dynamically assemble either gene-activating (YY1:BRDs/HATs) or re-

pressive (YY1:PRC2/HDACs) complexes under different cellular contexts. It appears to be the case that the gene-activating function of YY1 takes over during the pathogenesis of CRPC.

In addition to serving as a transcriptional regulator through direct binding to consensus motifs (such as CCAT sites at the PFKP promoter), YY1 was recently shown to function as a three-dimensional (3D) genome 'organizer' through interaction with 3D-genome regulator such as CTCF, thereby mediating formation of looping between enhancer and promoter (38,67). Indeed, our YY1 ChIP-seq in prostate cancer also uncovered that ∼75% of its binding sites are located at potential intergenic or intragenic enhancers and the rest 25% are at promoters. Thus, additional study is warranted to understand the molecular details and complicity regarding the multifaceted role of YY1 in oncogenesis. It is conceivable that CRPC, a heterogeneous disease subject to step-wise genetic and epigenetic alterations, gains aggressive features, such as enhanced metabolism and growth advantages, partly via deregulation of YY1 and co-factors. A better understanding of CRPC biology shall aid in the improved therapies in future.

DATA AVAILABILITY

RNA-seq and ChIP-seq reads have been deposited to Gene Expression Omnibus (GEO) under accession number GSE153640. The matched input data of the same ligand-stripped and DHT-stimulated 22Rv1 cells were previously published by us (NCBI GEO #GSE94013) and used herein for normalization of 22Rv1 YY1 ChIP-seq datasets.

SUPPLEMENTARY DATA

Supplementary Data are available at NAR Online.

ACKNOWLEDGEMENTS

We thank the UNC core facilities, including Imaging Core, High-throughput Sequencing Facility (HTSF), Bioinformatics Core, Tissue Procurement Facility, Translational Pathology Laboratory, Tissue Culture Facility and Animal Studies Core for their professional assistance of this work. We graciously thank Drs Seto, Zhang, Kim, Zhou and Strahl for providing reagents and the members of Cai, Wang and Earp laboratories for the useful discussion and technical support.

Author contributions: C.X. performed most of the experiments. Y.-H.T. and W.G. conducted analysis of RNA-seq and public cancer datasets under the supervision of J.S.P., G.G.W. and L.C. And A.J.S., S.G.M., R.D.E. and S.D.B. performed proteomics analyses using mass spectrometry under the supervision of A.J.T. P.G. analyzed ChIP-seq data under the supervision of D.Z., G.G.W. and L.C. Y.X., L.X. and J.H. provided critical tissue arrays and guidance on YY1 IHC. C.X., Y.W., J.H., D.Z., H.S.E., G.G.W. and L.C. interpreted the data. G.G.W. and L.C. conceived the idea, co-supervised the work and designed the research. C.X., G.G.W. and L.C. wrote the manuscript with input from all coauthors.

FUNDING

University of Arkansas for Medical Sciences Proteomics Core Facility; IDeA National Resource for Proteomics; Translational Research Institute through the National Center for Advancing Translational Sciences of the National Institutes of Health; Center for Translational Pediatric Research Bioinformatics Core Resource [TL1TR003109, P20GM121293, P20GM103625, P20GM103429, S10OD018445, UL1TR003107, R01CA236209]; UCRF Stimulus Initiative Grant of UNC Lineberger Cancer Center (to L.C., in part); UNC Cancer Center are supported in part by the UNC Lineberger Comprehensive Cancer Center Core Support Grant [P30-CA016086]; G.G.W. is an American Cancer Society (ACS) Research Scholar and a Leukemia and Lymphoma Society (LLS) Scholar.. Funding for open access charge: UCRF Stimulus Initiative Grant of UNC Lineberger Cancer Center (to L.C.).

Conflict of interest statement. J.H. is a consultant for or owns shares in the following companies: Kingmed, MoreHealth, OptraScan, Genetron, Omnitura, Vetonco, York Biotechnology, Genecode and Sisu Pharma. G.G.W. is an inventor of a patent application filed by University of North Carolina at Chapel Hill. G.G.W. received research fund from the Deerfield Management/Pinnacle Hill Company.

REFERENCES

1. Watson,P.A., Arora,V.K. and Sawyers,C.L. (2015) Emerging mechanisms of resistance to androgen receptor inhibitors in prostate cancer. *Nat. Rev. Cancer*, **15**, 701–711.
2. Gordon,S., Akopyan,G., Garban,H. and Bonavida,B. (2006) Transcription factor YY1: structure, function, and therapeutic implications in cancer biology. *Oncogene*, **25**, 1125–1142.
3. Shi,Y., Seto,E., Chang,L.S. and Shenk,T. (1991) Transcriptional repression by Yy1, a human Gli-Kruppel-related protein, and relief of repression by adenovirus E1a protein. *Cell*, **67**, 377–388.
4. Seto,E., Shi,Y. and Shenk,T. (1991) Yy1 is an initiator sequence-binding protein that directs and activates transcription invitro. *Nature*, **354**, 241–245.
5. Sarvagalla,S., Kolapalli,S.P. and Vallabhapurapu,S. (2019) The two sides of YY1 in cancer: a friend and a foe. *Front. Oncol.*, **9**, 1230.
6. Donohoe,M.E., Zhang,X.L., McGinnis,L., Biggers,J., Li,E. and Shi,Y. (1999) Targeted disruption of mouse Yin Yang 1 transcription factor results in peri-implantation lethality. *Mol. Cell. Biol.*, **19**, 7237–7244.
7. Meliala,I.T.S., Hosea,R., Kasim,V. and Wu,S. (2020) The biological implications of Yin Yang 1 in the hallmarks of cancer. *Theranostics*, **10**, 4183–4200.
8. Cairns,R.A., Harris,I.S. and Mak,T.W. (2011) Regulation of cancer cell metabolism. *Nat. Rev. Cancer*, **11**, 85–95.
9. Elia,I., Schmieder,R., Christen,S. and Fendt,S.M. (2016) Organ-specific cancer metabolism and its potential for therapy. *Handb. Exp. Pharmacol.*, **233**, 321–353.
10. Lin,C.C., Salzillo,T.C., Bader,D.A., Wilkenfeld,S.R., Awad,D., Pulliam,T.L., Dutta,P., Pudakalakatti,S., Titus,M., McGuire,S.E. *et al.* (2019) Prostate cancer energetics and biosynthesis. *Adv. Exp. Med. Biol.*, **1210**, 185–237.
11. Wang,J., Li,J.T., Li,X.J., Peng,S.B., Li,J., Yan,W.X., Cui,Y.B., Xiao,H.J. and Wen,X.Q. (2017) Increased expression of glycolytic enzymes in prostate cancer tissues and association with Gleason scores. *Int. J. Clin. Exp. Pathol.*, **10**, 11080–11089.
12. Eidelman,E., Twum-Ampofo,J., Ansari,J. and Siddiqui,M.M. (2017) The metabolic phenotype of prostate cancer. *Front. Oncol.*, **7**, 131.
13. Mor,I., Cheung,E.C. and Vousden,K.H. (2011) Control of glycolysis through regulation of PFK1: old friends and recent additions. *Cold Spring Harb. Symp. Quant. Biol.*, **76**, 211–216.

14. Lang,L., Chemmalakuzhy,R., Shay,C. and Teng,Y. (2019) PFKP signaling at a glance: an emerging mediator of cancer cell metabolism. *Rev. Biomarker Stud. Metab. Metab.-Related Disord.*, **1134**, 243–258.
15. Cai,L., Tsai,Y.H., Wang,P., Wang,J., Li,D.X., Fan,H.T., Zhao,Y.L., Bareja,R., Lu,R., Wilson,E.M. *et al.* (2018) ZFX mediates non-canonical oncogenic functions of the androgen receptor splice variant 7 in castrate-resistant prostate cancer. *Mol. Cell*, **72**, 341–354.
16. Filippakopoulos,P., Qi,J., Picaud,S., Shen,Y., Smith,W.B., Fedorov,O., Morse,E.M., Keates,T., Hickman,T.T., Felletar,I. *et al.* (2010) Selective inhibition of BET bromodomains. *Nature*, **468**, 1067–1073.
17. Ren,Z., Ahn,J.H., Liu,H., Tsai,Y.H., Bhanu,N.V., Koss,B., Allison,D.F., Ma,A., Storey,A.J., Wang,P. *et al.* (2019) PHF19 promotes multiple myeloma tumorigenicity through PRC2 activation and broad H3K27me3 domain formation. *Blood*, **134**, 1176–1189.
18. Fan,H., Lu,J., Guo,Y., Li,D., Zhang,Z.M., Tsai,Y.H., Pi,W.C., Ahn,J.H., Gong,W., Xiang,Y. *et al.* (2020) BAHCC1 binds H3K27me3 via a conserved BAH module to mediate gene silencing and oncogenesis. *Nat. Genet.*, **52**, 1384–1396.
19. Dobin,A., Davis,C.A., Schlesinger,F., Drenkow,J., Zaleski,C., Jha,S., Batut,P., Chaisson,M. and Gingeras,T.R. (2013) STAR: ultrafast universal RNA-seq aligner. *Bioinformatics*, **29**, 15–21.
20. Patro,R., Duggal,G., Love,M.I., Irizarry,R.A. and Kingsford,C. (2017) Salmon provides fast and bias-aware quantification of transcript expression. *Nat. Methods*, **14**, 417–419.
21. Love,M.I., Huber,W. and Anders,S. (2014) Moderated estimation of fold change and dispersion for RNA-seq data with DESeq2. *Genome Biol.*, **15**, 550.
22. Li,H. and Durbin,R. (2010) Fast and accurate long-read alignment with Burrows-Wheeler transform. *Bioinformatics*, **26**, 589–595.
23. Zhang,Y., Liu,T., Meyer,C.A., Eeckhoute,J., Johnson,D.S., Bernstein,B.E., Nussbaum,C., Myers,R.M., Brown,M., Li,W. *et al.* (2008) Model-based analysis of ChIP-Seq (MACS). *Genome Biol.*, **9**, R137.
24. Ye,T., Krebs,A.R., Choukrallah,M.A., Keime,C., Plewniak,F., Davidson,I. and Tora,L. (2011) seqMINER: an integrated ChIP-seq data interpretation platform. *Nucleic Acids Res.*, **39**, e35.
25. Heinz,S., Benner,C., Spann,N., Bertolino,E., Lin,Y.C., Laslo,P., Cheng,J.X., Murre,C., Singh,H. and Glass,C.K. (2010) Simple combinations of lineage-determining transcription factors prime cis-regulatory elements required for macrophage and B cell identities. *Mol. Cell*, **38**, 576–589.
26. Xu,B.W., On,D.M., Ma,A.Q., Parton,T., Konze,K.D., Pattenden,S.G., Allison,D.F., Cai,L., Rockowitz,S., Liu,S.C. *et al.* (2015) Selective inhibition of EZH2 and EZH1 enzymatic activity by a small molecule suppresses MLL-rearranged leukemia. *Blood*, **125**, 346–357.
27. Roux,K.J., Kim,D.I., Burke,B. and May,D.G. (2018) BioID: a screen for protein-protein interactions. *Curr. Protoc. Protein Sci.*, **91**, 19 23 1–19 23 15.
28. Roux,K.J., Kim,D.I. and Burke,B. (2013) BioID: a screen for protein-protein interactions. *Curr. Protoc. Protein Sci,*. **74**, 19 23 1–19 23 14.
29. Singh,D., Febbo,P.G., Ross,K., Jackson,D.G., Manola,J., Ladd,C., Tamayo,P., Renshaw,A.A., D'Amico,A.V., Richie,J.P. *et al.* (2002) Gene expression correlates of clinical prostate cancer behavior. *Cancer Cell*, **1**, 203–209.
30. Tomlins,S.A., Mehra,R., Rhodes,D.R., Cao,X.H., Wang,L., Dhanasekaran,S.M., Kalyana-Sundaram,S., Wei,J.T., Rubin,M.A., Pienta,K.J. *et al.* (2007) Integrative molecular concept modeling of prostate cancer progression. *Nat. Genet.*, **39**, 41–51.
31. Wu,S., Shi,Y., Mulligan,P., Gay,F., Landry,J., Liu,H., Lu,J., Qi,H.H., Wang,W., Nickoloff,J.A. *et al.* (2007) A YY1-INO80 complex regulates genomic stability through homologous recombination-based repair. *Nat. Struct. Mol. Biol.*, **14**, 1165–1172.
32. Handoko,L., Kaczkowski,B., Hon,C.C., Lizio,M., Wakamori,M., Matsuda,T., Ito,T., Jeyamohan,P., Sato,Y., Sakamoto,K. *et al.* (2018) JQ1 affects BRD2-dependent and independent transcription regulation without disrupting H4-hyperacetylated chromatin states. *Epigenetics*, **13**, 410–431.
33. Filippakopoulos,P., Qi,J., Picaud,S., Shen,Y., Smith,W.B., Fedorov,O., Morse,E.M., Keates,T., Hickman,T.T., Felletar,I. *et al.* (2010) Selective inhibition of BET bromodomains. *Nature*, **468**, 1067–1073.
34. Roe,J.S., Mercan,F., Rivera,K., Pappin,D.J. and Vakoc,C.R. (2015) BET bromodomain inhibition suppresses the function of hematopoietic transcription factors in acute myeloid leukemia. *Mol. Cell*, **58**, 1028–1039.
35. Cheung,K.L., Zhang,F., Jaganathan,A., Sharma,R., Zhang,Q., Konuma,T., Shen,T., Lee,J.Y., Ren,C., Chen,C.H. *et al.* (2017) Distinct roles of Brd2 and Brd4 in potentiating the transcriptional program for Th17 cell differentiation. *Mol. Cell*, **65**, 1068–1080.
36. Xu,Y. and Vakoc,C.R. (2017) Targeting cancer cells with BET bromodomain inhibitors. *Cold Spring Harb. Perspect. Med.*, **7**, a026674.
37. Wu,S.Y. and Chiang,C.M. (2007) The double bromodomain-containing chromatin adaptor Brd4 and transcriptional regulation. *J. Biol. Chem.*, **282**, 13141–13145.
38. Beagan,J.A., Duong,M.T., Titus,K.R., Zhou,L.D., Cao,Z.D., Ma,J.J., Lachanski,C.V., Gillis,D.R. and Phillips-Cremins,J.E. (2017) YY1 and CTCF orchestrate a 3D chromatin looping switch during early neural lineage commitment. *Genome Res.*, **27**, 1139–1152.
39. Yao,Y.L., Yang,W.M. and Seto,E. (2001) Regulation of transcription factor YY1 by acetylation and deacetylation. *Mol. Cell. Biol.*, **21**, 5979–5991.
40. Lin,W., Zhang,Z., Chen,C.H., Behringer,R.R. and Dent,S.Y. (2008) Proper Gcn5 histone acetyltransferase expression is required for normal anteroposterior patterning of the mouse skeleton. *Dev. Growth Differ.*, **50**, 321–330.
41. Helmlinger,D., Papai,G., Devys,D. and Tora,L. (2021) What do the structures of GCN5-containing complexes teach us about their function? *Biochim. Biophys. Acta Gene Regul. Mech.*, **1864**, 194614.
42. Varambally,S., Cao,Q., Mani,R.S., Shankar,S., Wang,X.S., Ateeq,B., Laxman,B., Cao,X.H., Jing,X.J., Ramnarayanan,K. *et al.* (2008) Genomic loss of microRNA-101 leads to overexpression of histone methyltransferase EZH2 in cancer. *Science*, **322**, 1695–1699.
43. Beltran,H., Prandi,D., Mosquera,J.M., Benelli,M., Puca,L., Cyrta,J., Marotz,C., Giannopoulou,E., Chakravarthi,B.V., Varambally,S. *et al.* (2016) Divergent clonal evolution of castration-resistant neuroendocrine prostate cancer. *Nat. Med.*, **22**, 298–305.
44. Alexander,K.E. and Rizkallah,R. (2017) Aurora A phosphorylation of YY1 during mitosis inactivates its DNA binding activity. *Sci. Rep.*, **7**, 10084.
45. Bushmeyer,S., Park,K. and Atchison,M.L. (1995) Characterization of functional domains within the multifunctional transcription factor, Yy1. *J. Biol. Chem.*, **270**, 30213–30220.
46. Lee,J.S., See,R.H., Galvin,K.M., Wang,J. and Shi,Y. (1995) Functional interactions between YY1 and adenovirus E1A. *Nucleic Acids Res.*, **23**, 925–931.
47. Shen,J., Jin,Z., Lv,H., Jin,K., Jonas,K., Zhu,C. and Chen,B. (2020) PFKP is highly expressed in lung cancer and regulates glucose metabolism. *Cell Oncol (Dordr)*, **43**, 617–629.
48. Allouche,A., Nolens,G., Tancredi,A., Delacroix,L., Mardaga,J., Fridman,V., Winkler,R., Boniver,J., Delvenne,P. and Begon,D.Y. (2008) The combined immunodetection of AP-2 alpha and YY1 transcription factors is associated with ERBB2 gene overexpression in primary breast tumors. *Breast Cancer Res.*, **10**, R9.
49. Zhang,J.J., Zhu,Y., Yang,C., Liu,X., Peng,Y.P., Jiang,K.R., Miao,Y. and Xu,Z.K. (2016) Yin Yang-1 increases apoptosis through Bax activation in pancreatic cancer cells. *Oncotarget*, **7**, 28498–28509.
50. Baritaki,S., Chatzinikola,A.M., Vakis,A.F., Soulitzis,N., Karabetsos,D.A., Neonakis,I., Bonavida,B. and Spandidos,D.A. (2009) YY1 over-expression in human brain gliomas and meningiomas correlates with TGF-1, IGF-1 and FGF-2 mRNA Levels. *Cancer Invest.*, **27**, 184–192.
51. Chinnappan,D., Xiao,D.M., Ratnasari,A., Andry,C., King,T.C. and Weber,H.C. (2009) Transcription factor YY1 expression in human gastrointestinal cancer cells. *Int. J. Oncol.*, **34**, 1417–1423.
52. Varum,S., Baggiolini,A., Zurkirchen,L., Atak,Z.K., Cantu,C., Marzorati,E., Bossart,R., Wouters,J., Hausel,J., Tuncer,E. *et al.* (2019) Yin Yang 1 orchestrates a metabolic program required for both neural crest development and melanoma formation. *Cell Stem Cell*, **24**, 637–653.
53. Zurkirchen,L., Varum,S., Giger,S., Klug,A., Hausel,J., Bossart,R., Zemke,M., Cantu,C., Atak,Z.K., Zamboni,N. *et al.* (2019) Yin Yang 1 sustains biosynthetic demands during brain development in a stage-specific manner. *Nat. Commun.*, **10**, 2192.

54. Li,Y., Kasim,V., Yan,X., Li,L., Meliala,I.T.S., Huang,C., Li,Z., Lei,K., Song,G., Zheng,X. *et al.* (2019) Yin Yang 1 facilitates hepatocellular carcinoma cell lipid metabolism and tumor progression by inhibiting PGC-1beta-induced fatty acid oxidation. *Theranostics*, **9**, 7599–7615.
55. Chen,F., Zhou,J., Li,Y., Zhao,Y., Yuan,J., Cao,Y., Wang,L., Zhang,Z., Zhang,B., Wang,C.C. *et al.* (2019) YY1 regulates skeletal muscle regeneration through controlling metabolic reprogramming of satellite cells. *EMBO J.*, **38**, e99727.
56. Park,A., Lee,J., Mun,S., Kim,D.J., Cha,B.H., Moon,K.T., Yoo,T.K. and Kang,H.G. (2017) Identification of transcription factor YY1 as a regulator of a prostate cancer-specific pathway using proteomic analysis. *J. Cancer*, **8**, 2303–2311.
57. Cunningham,J.T., Rodgers,J.T., Arlow,D.H., Vazquez,F., Mootha,V.K. and Puigserver,P. (2007) mTOR controls mitochondrial oxidative function through a YY1-PGC-1alpha transcriptional complex. *Nature*, **450**, 736–740.
58. Wu,S., Wang,H., Li,Y., Xie,Y., Huang,C., Zhao,H., Miyagishi,M. and Kasim,V. (2018) Transcription factor YY1 promotes cell proliferation by directly activating the pentose phosphate pathway. *Cancer Res.*, **78**, 4549–4562.
59. Umar,S.M., Kashyap,A., Kahol,S., Mathur,S.R., Gogia,A., Deo,S.V.S. and Prasad,C.P. (2020) Prognostic and therapeutic relevance of phosphofructokinase platelet-type (PFKP) in breast cancer. *Exp. Cell Res.*, **396**, 112282.
60. Lang,L., Chemmalakuzhy,R., Shay,C. and Teng,Y. (2019) PFKP signaling at a glance: an emerging mediator of cancer cell metabolism. *Adv. Exp. Med. Biol.*, **1134**, 243–258.
61. Kim,N.H., Cha,Y.H., Lee,J., Lee,S.H., Yang,J.H., Yun,J.S., Cho,E.S., Zhang,X., Nam,M., Kim,N. *et al.* (2017) Snail reprograms glucose metabolism by repressing phosphofructokinase PFKP allowing cancer cell survival under metabolic stress. *Nat. Commun.*, **8**, 14374.
62. Guo,Y., Zhao,S. and Wang,G.G. (2021) Polycomb gene silencing mechanisms: PRC2 chromatin targeting, H3K27me3 'Readout', and phase separation-based compaction. *Trends Genet.*, doi:10.1016/j.tig.2020.12.006.
63. Hoxha,S., Shepard,A., Troutman,S., Diao,H., Doherty,J.R., Janiszewska,M., Witwicki,R.M., Pipkin,M.E., Ja,W.W., Kareta,M.S. *et al.* (2020) YAP-mediated recruitment of YY1 and EZH2 represses transcription of key cell-cycle regulators. *Cancer Res.*, **80**, 2512–2522.
64. Du,J., Kirk,B., Zeng,J., Ma,J. and Wang,Q. (2018) Three classes of response elements for human PRC2 and MLL1/2-Trithorax complexes. *Nucleic. Acids. Res.*, **46**, 8848–8864.
65. Zhou,L., Sun,K., Zhao,Y., Zhang,S., Wang,X., Li,Y., Lu,L., Chen,X., Chen,F., Bao,X. *et al.* (2015) Linc-YY1 promotes myogenic differentiation and muscle regeneration through an interaction with the transcription factor YY1. *Nat. Commun.*, **6**, 10026.
66. Lu,Z., Hong,C.C., Kong,G., Assumpcao,A., Ong,I.M., Bresnick,E.H., Zhang,J. and Pan,X. (2018) Polycomb group protein YY1 is an essential regulator of hematopoietic stem cell quiescence. *Cell Rep.*, **22**, 1545–1559.
67. Weintraub,A.S., Li,C.H., Zamudio,A.V., Sigova,A.A., Hannett,N.M., Day,D.S., Abraham,B.J., Cohen,M.A., Nabet,B., Buckley,D.L. *et al.* (2017) YY1 is a structural regulator of enhancer-promoter loops. *Cell*, **171**, 1573–1588.